ROYAL SOCIETY OF CHEMISTRY

PAPER

Check for updates

Mono- and bimetallic homo- and heterodinuclear Pd and Pt complexes bridged by diphosphines: synthesis, characterisation and cytotoxicity

Basile Roufosse, [ID] [a] Tomas Brice,[a] Marco Papaldo,[a] Lucy W. Macharia,[b] Karabo Serala,[b] Mihlali V. Mlaza,[b] Thato T. Medupe,[b] Sharon Prince, [ID] *[b] Christoph Marschner, [ID] [c] Thomas J. Cleij [ID] [a] and Burgert Blom [ID] *[b]

Herein we report a series of monometallic complexes: [(κ^2-dppe)MCl(κ^1-dppx)](OTf) (where dppe = 1,2-bis(diphenylphosphino)ethane; dppx = 1,4-bis(diphenylphosphino)butane (dppb) (M = Pd (**Pd-1**) or Pt (**Pt-1**)), 1,5-bis(diphenylphosphino)pentane (dpppent) (M = Pd (**Pd-2**) or Pt (**Pt-2**)), or 1,6-bis(diphenylphosphino)hexane (dpph) (M = Pd (**Pd-3**) or Pt (**Pt-3**))). We also report the homobimetallic complexes [((κ^2-dppe)PdCl)$_2$(μ-dppx)](2OTf) (dppx = dppb (**PdPd-1**), dpppent (**PdPd-2**) or dpph (**PdPd-3**)). In addition, the Ru(II)-based heterobimetallic complexes [(κ^2-dppe)ClM(μ-dppx)RuCl$_2$(η^6-p-cym)](OTf) (M = Pd and dppx = dppb (**PdRu-1**), M = Pd and dppx = dpppent (**PdRu-2**), M = Pd and dppx = dpph (**PdRu-3**), M = Pt and dppx = dppb (**PtRu-1**), M = Pt and dppx = dpppent (**PtRu-2**), M = Pt and dppx = dpph (**PtRu-3**), and Os-based heterobimetallic complexes [(κ^2-dppe)ClPd(μ-dppx)OsCl$_2$(η^6-p-cym)](OTf) (dppx = dppb (**PdOs-1**), dpppent (**PdOs-2**) and dpph (**PdOs-3**)) are also reported. All complexes were fully characterised by spectroscopic means and their stability in DMSO was determined via time-dependent NMR spectroscopy. Aquation studies were performed in a PBS buffer : DMSO solution (90 : 10 v/v) at 37 °C to determine the various entities which could form in biological media and are discussed. The solid-state structures of complexes **PdPd-0**, **PdPd-1** and **PdRu-1** were further characterised by single crystal X-ray diffraction analyses and are reported. The cytotoxicity of all complexes was evaluated in vitro against a wide panel of cancer cell lines. While the monometallic and homobimetallic complexes showed sub-optimal activity, the heterobimetallic complexes all displayed good to excellent cytotoxicity. **PdRu-1** displayed an IC$_{50}$ value of 3.43 ± 1.43 μM and a selectivity index of 6.16 on the Ca Ski cell line. The results from this study highlight the increased efficacy of heterobimetallic systems with regards to their monometallic or homobimetallic counterparts for Pd(II) and Pt(II) type complexes.

[a]Maastricht Science Programme, Faculty of Science and Engineering, Maastricht University, Paul-Henri Spaaklaan 1, 6229 EN, Maastricht, The Netherlands
[b]Department of Human Biology, Cell Biology Division, University of Cape Town, Observatory, 7925, South Africa. E-mail: sharon.prince@uct.ac.za, burgert.blom@uct.ac.za
[c]Institut für Anorganische Chemie, Technische Universität Graz, Stremayrgasse 9, A-8010 Graz, Austria

Introduction

Cancer is one of the predominant health challenges in the world, with more than 2 million new cases and more than 600 000 deaths projected in 2025 in the United States alone.[1] The number of cases worldwide is predicted to reach 35 million by 2050, given the overall increase in population and life expectancy.[2] Pt-based drugs, which are linked to a plethora of side 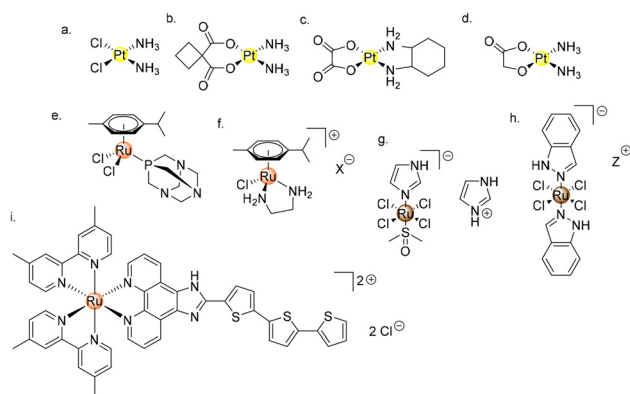effects, are still the forefront chemotherapeutic drugs (Scheme 1a–d).[3–8] However some Ru(II)-based complexes have been studied and are linked to promising results (Scheme 1e–i).[9–16] Another class of compounds which have been somewhat underexplored in comparison to the multitude of mononuclear complexes reported in the literature are bimetallic complexes. These compounds make use of two metals, where it can be further differentiated into the homobimetallic (same metals) or heterobimetallic (two different metals) class. The nature of the bridging ligand can be varied, and diphosphines have shown to be suitable for this purpose due to the simple finetuning of both steric and electronic properties.[17] Upon addition of a diphosphine to a halide-bridged dimer precursor, dimer cleavage and binding to the metal centre by the donor phosphine occurs readily to form a monomeric structure bearing a pendant P atom. This intermediate complex can then be used in a subsequent dimer-cleavage reaction, generating a homo- or heterobimetallic complex. We

Scheme 1 Chemical structures of complexes which reached human clinical trials. a: Cisplatin, b: carboplatin, c: oxaliplatin, d: nedaplatin, e. RAPTA-C, f. RAED-C, g: NAMI-A, h: KP1019 (Z = indazoleH$^+$), KP1339 (Z = Na$^+$), and i. TLD1433.

have recently reviewed all homo- and heteromultimetallic complexes with a group 8 metal bridged by diphosphines,[18] as well as Pd and Pt complexes of analogous motifs,[17] all complexes bridged by dppm (1,1-bis(diphenylphosphino)methane)[19] and osmium-based complexes bearing a η^6-arene and a phosphine co-ligand[20] involved in biological studies.

Bennet *et al.* have reported some examples of homobimetallic Pd(II) and Pt(II) complexes bridged by diphosphines and showed suboptimal activity of the Pd(II) examples compared to their Pt(II) analogues.[21] Another study has uncovered enhanced activity of a cyclometallated Pd(II)–(μ-dppe)–Pd(II) complex compared to cisplatin in a wide array of cell lines.[22] A more recent study reported encouraging cytotoxic activity of dinuclear palladacycles in MCF-7 and MDA-MB-231 cell lines, even though cisplatin was not used as control.[23] It is worth mentioning that some monometallic Pd(II) and Pt(II) complexes also displayed good to excellent cytotoxic activities against several cancer cell lines,[24–29] and several reviews highlight the relevance of monometallic complexes.[30–33] Homobimetallic complexes of the type [(η^6-arene)RuCl$_2$]$_2$ (μ-diphosphine) have been shown to be underwhelmingly active,[34,35] with the exception of two complexes reported by Klaimanee *et al.*, making use of the methyl-substituted diphosphines 1,2-bis(diphenylphosphino)propane and 2,4-bis(diphenylphosphino)pentane, which displayed considerably higher cytotoxic activities than cisplatin.[36]

Several accounts report increased cytotoxic activity in line with the heterobimetallic nature of the complexes studied. In fact, some examples of Pt(II)–(μ-dppm)–Au(I) complexes were reported to be more effective than their monometallic Pt(II) precursors.[37] In addition, previous research conducted by us on monometallic Fe(II) and their analogous heterobimetallic Fe(II)–Ru(II) complexes showed that the bimetallic examples displayed higher level of DNA interactions and their cytotoxic activities were found similar to that of cisplatin on the cell lines tested.[38] We also reported increased activity of [(η^5-Cp)Fe (CO)I(μ-dppm)RuCl$_2$(η^6-arene)] (where arene = *p*-cymene or

C$_6$H$_6$) compared to homobimetallic [(η^6-C$_6$H$_6$)RuCl$_2$]$_2$(μ-dppm),[35] and some comprehensive reviews highlight multiple heterobimetallic complexes with various ligand scaffolds and their anticancer activities.[39,40]

As part of our ongoing research programme into the development and anticancer testing of bimetallic complexes, with a view to establish a large library of compounds for further biological studies, we report herein eighteen novel complexes subdivided in three categories: (a) monometallic Pd or Pt-based complexes bearing a κ^1-diphosphine with the general formula [(κ^2-dppe)MCl(κ^1-dppx)](OTf), where dppx = 1,4-bis(diphenylphosphino)butane (dppb), 1,5-bis(diphenylphosphino)pentane (dpppent), or 1,6-bis(diphenylphosphino)hexane (dpph) and M = Pd or Pt; (b) homobimetallic Pd-based complexes bridged by a diphosphine with the general formula [((κ^2-dppe)PdCl)$_2$(μ-dppx)](2OTf); and (c) heterobimetallic complexes of the type [(κ^2-dppe)ClM(μ-dppx)RuCl$_2$(*p*-cym)] (where M = Pd or Pt), and [(κ^2-dppe)ClPd(μ-dppx)OsCl$_2$(*p*-cym)](OTf) (Fig. 1). The rationale behind this collection of complexes is to evaluate multiple aspects in the drug design process: Firstly, analogous complexes of which the only structural difference stems from one same group transition metal (*i.e.* Pd(II) *vs.* Pt(II), Ru(II) *vs.* Os(II)) are tested to determine which is most active. Secondly, as seen in multiple reports, monometallic complexes tend to be less active than their bimetallic counterparts, as well as homobimetallic complexes displaying less activity than their heterobimetallic complexes.[18] Hence, the monomer precursors and homobimetallic complexes were also evaluated to further test these observations. Thirdly, a previous study reported by us has seen a correlation between spacer length (*i.e.* number of CH$_2$ groups within the bridging ligand backbone) and cytotoxic activity.[38] Hence, the length of the diphosphine spacer chain was varied systematically for all classes of compounds reported herein to evaluate whether this trend can be observed in the three different types of complexes. All complexes were characterised spectroscopically, three of which were further characterised by single crystal X-ray diffraction analysis. Rates of aquation and tentative speciation were derived for selected examples in a PBS buffer : DMSO solution (90 : 10 v/v) and are presented. The cell viability was evaluated on eight human cancer cell lines, including cervical (HeLa and Ca Ski), pan-
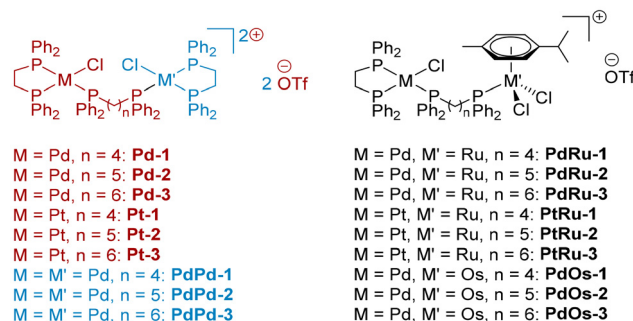
Fig. 1 Schematic representation of the complexes discussed herein, and their respective labels.

creatic (PANC-1 and CFPAC-1), rhabdomyosarcoma (RD and RH30), and breast (MCF-7 and MDA-MB-231). The most effective compounds were also tested against non-malignant MRC-5 cell line. The IC_{50} values of the two best-performing complexes were determined on cervical and pancreatic cancer cell lines, and their selectivity indices were derived by cross-testing on FG0 non-malignant cells.

Results and discussion

### Synthesis and spectroscopic properties of precursor dimer complexes PdPd-0 and PtPt-0

Dimer complexes similar in structure as **PdPd-0** have been previously reported in the literature,[41–45] with the first example dating back to 1979.[41] However, these complexes contained either ClO_4 or BF_4 counteranions. Herein we report the synthesis of an analogous dimer complex containing the triflate (SO_3CF_3) counteranion. The dimer precursor was synthesised using adapted methods,[46] by mixing [(dppe)PdCl$_2$] with AgOTf in dichloromethane at room temperature (Scheme 2). The desired product was isolated in good yields (75%) as an air stable solid. Interestingly, the dimer exhibited different reactivities towards deuterated solvents upon NMR analysis (Scheme 3). In fact, in $CDCl_3$, a signal corresponding to [(dppe)PdCl$_2$] starting material progressively increases in intensity over time in the $^{31}P\{^1H\}$ NMR spectrum, revealing chlorination at Pd(II) in $CDCl_3$. However, in DMSO-d_6, dimer cleavage to form the DMSO adduct is observed through the appearance of two sets of doublets in the $^{31}P\{^1H\}$ NMR spectrum (δ = 70.9 and 69.0 ppm), corresponding to the chemically inequivalent P atoms of dppe upon DMSO binding to the Pt(II) centre. In acetone-d_6, a singlet signal is observed at δ = 76.9 ppm in the $^{31}P\{^1H\}$ NMR spectrum, supporting the chemical equivalence of each P atom within the structure, as well as

a doublet signal in the aliphatic region in the $^{13}C\{^1H\}$ NMR spectrum, corresponding to the C atoms within the dppe backbone (Fig. S1 and S20). In addition, a singlet signal can be observed at δ = −77.6 ppm in the ^{19}F NMR spectrum, confirming the presence of the triflate anions. Crystals suitable for X-ray diffraction analyses were grown through slow evaporation of a concentrated dichloromethane solution at 4 °C and the structure is reported in the SI (Fig. S193). The synthesis of **PtPt-0** was optimised compared to previous reports.[47] The precursor complex [(dppe)PtCl$_2$] is obtained via reaction of [(COD)PtCl$_2$] and dppe in dichloromethane.[48] The intermediate monomer complex is subsequently reacted with AgOTf in dichloromethane at room temperature for 1.5 h in the absence of light, yielding the desired dimer complex **PtPt-0** in 70% yield (Scheme 2).

Synthesis and spectroscopic properties of monometallic precursor complexes Pd-x and Pt-x (x = 1, 2 or 3)

The monometallic complexes **Pd-x** and **Pt-x** were synthesised through slow addition of a solution containing the respective dimer precursors **PdPd-0** or **PtPt-0** to another solution containing two equivalents of the respective diphosphine ligands (1,4-bis(diphenylphosphino)butane (dppb, **Pd-1** or **Pt-1**), 1,5-bis(diphenylphosphino)pentane (dpppent, **Pd-2** or **Pt-2**) and 1,6-bis(diphenylphosphino)hexane (dpph, **Pd-3** or **Pt-3**)) in dichloromethane (Scheme 4). The slow addition of the dimer complex prevents the formation of dinuclear species where each P atoms on the ligand would bind to a different Pd(II)/Pt(II) centre. Reactions attempted with shorter chain length diphosphines (dppm, dppe or dppp) resulted in the formation of the desired products as well as a cyclic side-product where the diphosphine bound in a κ^2 fashion to the M(II) centre. The mononuclear complexes were obtained in good yields (65–81%) as pale-yellow powders, stable in air for extended periods of time.

FT-IR spectroscopy revealed very similar spectra along all monometallic complexes, with C–H stretching vibrations observed in the range of 3100–2800 cm^{-1} being the only assignable signals (Fig. S103–S108). The UV-Vis spectra of **Pd-x** were very similar to one another, with the main features being an intense absorption at 226 nm, a shoulder at 270 nm and a minor absorption at 331 nm (Fig. S125–S127). In **Pt-3**, the shoulder shifted to 274 nm, and no absorption was observed at 331 nm (Fig. S129). ^1H NMR spectra revealed a doublet signal in the aliphatic region in all six cases, corresponding to
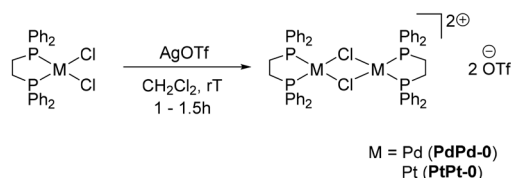
Scheme 2 Synthesis of the dimer precursors **PdPd-0** and **PtPt-0**.
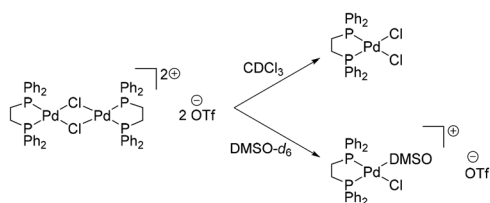
Scheme 3 Decomposition products observed in solution upon NMR analysis of **PdPd-0** in different solvents.
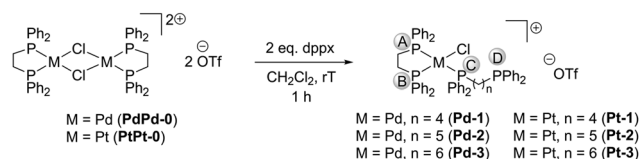
Scheme 4 Synthesis of the monometallic complexes **Pd-x** and **Pt-x** (x = 1, 2 or 3). The letters circled in grey represent the labeling of the P atoms used in-text.

the κ^2-dppe ethylene bridgehead protons. Additional sets of multiplets in the aromatic region, as well as extra signals in the aliphatic region confirmed the binding of the diphosphine ligand to the Pd(II) centre. The aromatic signals integrate to 40 H, corresponding to the four Ph rings attached to P, whereas the aliphatic protons of the tether integrate to the expected values in all three cases (Fig. S2–S7). Further proof of the binding of diphosphine in a κ^1-fashion to Pd(II) was revealed by the $^{31}P\{^1H\}$ NMR spectra: an upfield singlet signal is observed corresponding to the pendant P atom. The three P atoms bound to Pd(II) or Pt(II) were all displayed as doublet of doublets. P^A and P^C exhibit large *trans*-coupling to each other, while P^B exhibits smaller *cis*-couplings to P^A and P^C (see Scheme 4 for atoms labelling) (Fig. S39–S44). These complexes exist as conformers in solution, as can be seen especially in the P^C signal, which displays two sets of doublet of doublets. This is not uncommon for such complexes, as conformational changes were observed in other phosphine-containing complexes.[49–53] DMSO-stability studies performed *via* ^1H and ^{31}P NMR spectroscopy in DMSO-d_6 revealed that the complexes maintain their structural integrity in solution over time (Fig. S67–S78). ESI-TOF-MS confirmed the presence of the expected complexes, as the molecular peak of the cation was observed in all cases, with the expected isotope pattern (Fig. S155–S160). Complexes **Pd-3** and **Pt-x** (x = 1, 2 or 3) also displayed an $[M + O]^+$ fragment, likely due to oxidation at the pendant P, which is typical of such complexes under ESI-MS ionisation conditions.[38]

### Synthesis and spectroscopic properties of homobimetallic complexes PdPd-x (x = 1, 2 or 3)

The syntheses of the homodinuclear complexes **PdPd-x** (x = 1, 2 or 3) were carried out by reacting the dimer precursor **PdPd-0** with the respective diphosphine in a 1 : 1 equivalent in dichloromethane to selectively afford through dimer-cleavage the desired bimetallic complexes in good yields (Scheme 5). Binding of the diphosphine in a µ-fashion was confirmed through the absence of the upfield singlet in the $^{31}P\{^1H\}$ NMR spectrum, which is observed in the case of complexes **Pd-x** and **Pt-x** bearing the pendant P atom. On the other hand, three resonance signals are observed, corresponding to Pd-bound P^A, P^B and P^C (Fig. S45–S47). The ^1H NMR spectra are distinct from **Pd-x**, as the homobimetallic systems are symmetrical. The aromatic region integrates to 60 protons, in line with the presence of a second κ^2-dppe moiety. The aliphatic region dis-

plays two signals assignable to the κ^2-dppe moiety, each integrating to four protons. In addition, resonance signals assigned to the dppx bridging ligand are also observed, with the respective integration values matching depending on the ligand length (Fig. S8–S10). A singlet peak at δ = −77.7 ppm in the ^{19}F NMR spectrum corresponds to the presence of the triflate anion. Similar to the mononuclear complexes, the homobimetallic complexes displayed good stability in DMSO-d_6, as no noticeable change was observed in the ^1H and ^{31}P NMR spectra over a 180 minutes period (Fig. S79–S84). ESI-MS confirmed the formation of the desired products through the $[M\text{-OTf}]^+$ peak with expected isotope pattern in all cases (Fig. S161–S163). The UV-Vis spectra exhibit very similar features as the monometallic complexes **Pd-x**, with an intense absorption around 225 nm, followed by a clear shoulder at 265 nm and a lower absorption around 335 nm (Fig. S131, S133 and S135).

Synthesis and characterisation of the heterobimetallic complexes PdRu-x, PtRu-x and PdOs-x (x = 1, 2 or 3)

The heterodinuclear complexes were synthesised in similar fashion, through the addition of dimer precursors $[[(p\text{-cym})MCl_2]_2$ (M = Ru(II), Os(II)) to a solution of the respective monometallic complexes **Pd-x** or **Pt-x** in dichloromethane and stirring at room temperature for 1.5 to 2 hours (Schemes 6 and 7).

The complexes were obtained as orange to brick-red powders in good yields (61 to 85%) and are air stable over extended periods of time. The ^1H NMR spectra of all complexes showed similar signals compared to the monometallic counterparts, with the addition of extra resonance signals corresponding to the 4H of the *p*-cymene moiety, a doublet corresponding to the CH_3 groups of the isopropyl unit, as well as a singlet peak corresponding to the CH_3 on *p*-cymene ring. The expected septet from methine CH could not be observed due to overlapping signals from the alkyl chain of the bridging ligand, nevertheless its presence was determined through ^1H–^1H 2D COSY NMR experiments (Fig. S11–S19). $^{13}C\{^1H\}$ NMR spectroscopy further corroborated the incorporation of Ru(II)/Os(II) into the structure, with seven extra signals observed, in line with the seven distinct C atoms present within the *p*-cymene moiety (Fig. S29–S37). In the case of **PdRu-x** and **PtRu-x**, binding of Ru(II) was further confirmed by the presence of a lowfield shifted resonance signal in the $^{31}P\{^1H\}$ NMR spectrum, in comparison to the precursors bearing a pendant P atom. This observation is not the case for **PdOs-x**, as the signal remains upfield, in line with the greater shielding effect of Os(II) compared to Ru(II) (Fig. S48–S56). The presence of conformers was observed in all heterobimetallic complexes. In order to further corroborate this, variable temperature NMR spectroscopic investigations was performed on **RuPt-3**, where coalescence of the P^C signals into a clear doublet of doublet was observed from 333 K on (Fig. 3), revealing the existence of conformers in solution. In line with the previously discussed **Pd-x**, **Pt-x** and **PdPd-x** series, the heterobimetallic complexes seem to maintain their structural integrity in DMSO-d_6 over time, as no obvious change in the ^1H and ^{31}P NMR spectra were observed (Fig. S85–S100). The formation of the desired
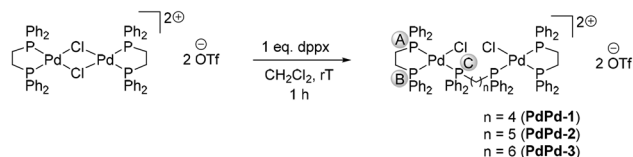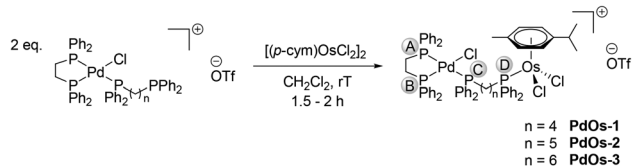

Scheme 5 Synthesis of the homobimetallic complexes **PdPd-x** (x = 1, 2 or 3). The letters circled in grey represent the labeling of the P atoms used in-text.
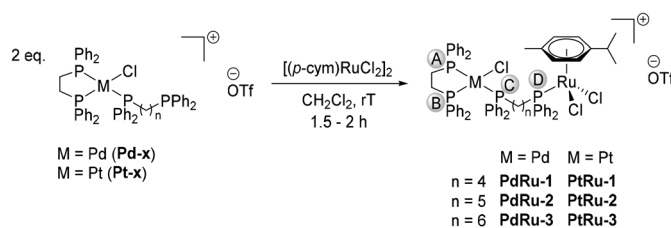
Scheme 6 Synthesis of the heterobimetallic complexes **PdRu-x** and **PtRu-x** (x = 1, 2 or 3). The letters circled in grey represent the labeling of the P atoms used in-text.


Scheme 7 Synthesis of the heterobimetallic complexes **PdOs-x** (x = 1, 2 or 3). The letters circled in grey represent the labeling of the P atoms used in-text.

products was further supported by ESI-MS, where the M$^+$ peak of all complexes was observed (Fig. 2 and Fig. S164–S178). Regarding UV-Vis spectroscopy, a clear difference can be observed when comparing the heterobimetallic complexes to the monometallic precursors and the homobimetallic complexes **PdPd-x**. In fact, discreet low intensity absorption maxima can be seen at higher concentrations, corresponding to symmetry forbidden electronic d–d transitions occurring at the Ru(II) or Os(II) centres (Fig. S137–S153).

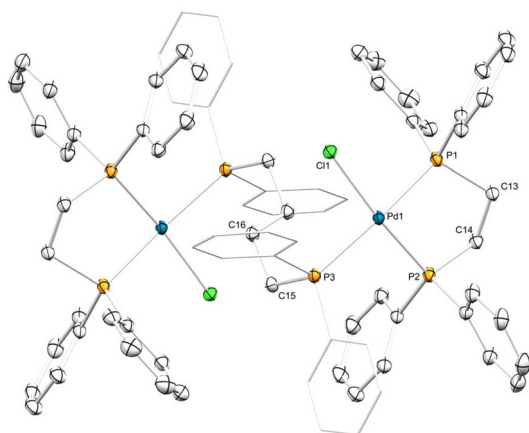### Single crystal X-ray diffraction investigations

Crystals of **PdPd-0**, **PdPd-1** and **PdRu-1**, suitable for X-ray diffraction analysis, were grown *via* slow evaporation of dichloromethane at 4 °C (**PdPd-0**), or slow diffusion of Et$_2$O into a concentrated solution of the respective complexes in dichloromethane at room temperature (**PdPd-1** and **PdRu-1**) and are the results are presented in Fig. 4–6.

The dimer complexes [(dppe)PdCl]$_2$(2ClO$_4$) and [(dppe)PdCl]$_2$(2BF$_4$) have previously been characterised *via* single
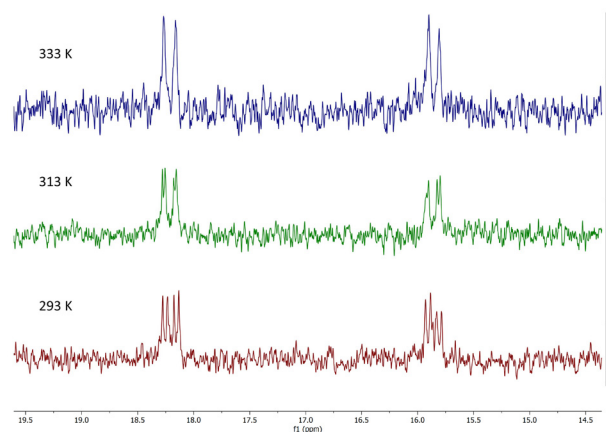
Fig. 3 Variable temperature $^{31}P\{^1H\}$ NMR studies of **PtRu-3**, zoomed in on P^C. The FID data was further processed with an exponential apodization function with a line broadening of 1 Hz in order to improve the signal to noise ratio.

Fig. 4 ORTEP representation of complex **PdPd-0** in the solid state determined by single crystal X-ray diffraction analysis. Thermal ellipsoids represented at the 30% probability level. H atoms and solvent molecule omitted for clarity. Selected bond lengths [Å]: Pd(1)−Cl(1) 2.4014(5), Pd(1)−Cl(1′) 2.4040(5), Pd(1)−P(1) 2.2257(6), Pd(1)−P(2) 2.2471(5). Selected bond angles [°]: P(1)−Pd(1)−Cl(1) 178.38(2), P(1)−Pd(1)−Cl(1′) 91.661(19), P(2)−Pd(1)−Cl(1′) 174.967(19), P(2)−Pd(1)−Cl(1) 96.039(19), P(2)−Pd(1)−P(1) 84.80(2).

Fig. 2 Stacked mass spectra of **PdOs-1** (bottom), **PdOs-2** (middle) and **PdOs-3** (top) zoomed in on the [M$^+$] peak.

crystal X-ray diffraction analysis.[44,45] Herein we report the solid state crystal structure of the analogous complex [(dppe) PdCl]$_2$(2OTf). **PdPd-0** crystallised in the triclinic crystal system

Fig. 5 ORTEP representation of the **PdPd-1** cation in the solid state determined by single crystal X-ray diffraction analysis. Thermal ellipsoids represented at the 30% probability level. H atoms and counteranions omitted for clarity. The phenyl rings of the bridging dppb entity are represented as wireframes for clarity. Selected bond lengths [Å]: Pd(1)−Cl(1) 2.3458(5), Pd(1)−P(1) 2.2980(6), Pd(1)−P(2) 2.2651(6), Pd(1)−P(3) 2.3734(6). Selected bond angles [°]: Cl(1)−Pd(1)−P(3) 89.78(2), P(1)−Pd(1)−Cl(1) 88.64(2), P(1)−Pd(1)−P(3) 175.60(2), P(2)−Pd(1)−Cl(1) 172.88(2), P(2)−Pd(1)−P(1) 85.14(2), P(2)−Pd(1)−P(3) 96.18(2).
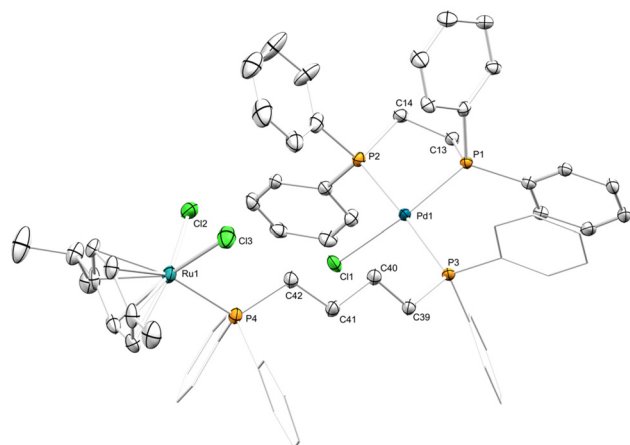
Fig. 6 ORTEP representation of the **PdRu-1** cation in the solid state determined by single crystal X-ray diffraction analysis. Thermal ellipsoids represented at the 30% probability level. H atoms and counteranion omitted for clarity. The phenyl rings of the bridging dppb entity are represented as wireframes for clarity. Selected bond lengths [Å]: Pd(1)−P(1) 2.2472(17), Pd(1)−Cl(1) 2.3401(18), Pd(1)−P(2) 2.3065(18), Pd(1)−P(3) 2.3493(18), Ru(1)−Cl(3) 2.419(3), Ru(1)−Cl(2) 2.412(3), Ru(1)−P(4) 2.344(2), Ru(1)−C(58) 2.208(8). Selected bond angles[°]: P(1)−Pd(1)−Cl(1) 169.33(7), P(1)−Pd(1)−P(2) 83.77(6), P(1)−Pd(1)−P(3) 98.87(6), Cl(1)−Pd(1)−P(3) 90.46(7), P(2)−Pd(1)−Cl(1) 86.79(7), P(2)−Pd(1)−P(3) 177.03(7), Cl(2)−Ru(1)−Cl(3) 88.03(11), P(4)−Ru(1)−Cl(3) 88.21(8), P(4)−Ru(1)−Cl(2) 84.21(8).

with the space group $P\bar{1}$ (Fig. 4). The cationic species has an inversion centre in between the two Pd atoms and presents strikingly similar features than the previously reported analogous structures, which is to be expected.

PdPd-1 crystallises in the monoclinic crystal system with the space group $P2_1/c$ (Fig. 5). The molecule bears an inversion centre between the two central C atoms of the bridging dppb ligand. The complex displays a distorted square planar geometry at Pd(II), with bond angles of 88.63° (Cl1–Pd1–P1), 85.14° (P1–Pd1–P2), 96.18° (P2–Pd1–P3) and 89.78° (P3–Pd1–Cl1). This is similar to the complex [(κ²-dppe)Pd(Ph)]₂(μ-dppe), reported by Zhuravel and co-workers, where the bond angle P2–Pd1–P3 was found to be 100.95°, whereas the remaining angles were all below 90°.[54] This large difference is likely due to steric strain between the phenyl rings on each P atoms. The main difference between the herein reported structure and that of Zhuravel *et al.* is the shorter Pd(1)–P(2) bond length in **PdPd-1**, due to the lesser electron donating abilities of Cl compared to Ph. Another noteworthy detail are the more obtuse bond angles around P(3) in the bridging dppb moiety compared to the free ligand. Indeed, while the bond angle between C(Ph)–P–C(Ph) remains similar between free dppb and **PdPd-1**, both C(Ph)–P–C(chain) angles average 105.51° in **PdPd-1**, where they average 101.54° in free dppb.[55] The complete crystal data for **PdPd-1** can be found in Tables S8–S15.

Complex **PdRu-1** crystallises in the monoclinic crystal system with the space group $P2_1/n$ (Fig. 6). The geometry and metrical parameters around Pd(II) is analogous to **PdPd-1** within narrow limits. The geometry around the Ru(II) centre is distorted octahedral, where the *p*-cymene unit occupies three binding sites, while the remaining ligands occupy the remaining three. This "piano-stool" configuration for Ru(II) is common and multiple examples of [(*p*-cym)RuCl₂(PPh₂R)] complexes have been characterised *via* X-ray diffraction analyses.[56–59] The complete crystal data for **PdRu-1** can be found in Tables S16–S22.

Cell viability studies

All complexes were tested at 10 μM *in vitro* against cervical cancer (HeLa and Ca Ski), pancreatic cancer (PANC-1 and CFPAC-1), rhabdomyosarcoma (RD and RH30), and breast cancer (MCF-7 and MDA-MB-231) cell lines, and one non-malignant cell line (MRC-5). The initial concentration of 10 μM was selected based on the National Cancer Institute (NCI, USA) screening protocol, which uses this threshold to identify compounds with promising anticancer activity.[60–62] Compounds that inhibit cell viability by more than 50% at this concentration are considered sufficiently active to warrant further investigation. The results are tabulated in Table 1 and the related plots can be found in the SI (Fig. S179–S183). The most notable results were observed on the two pancreatic cancer cell lines, where all heterobimetallic complexes reduced cell viability by more than 50%, as well as outperformed cisplatin. The two homobimetallic complexes **PdPd-1** and **PdPd-2** displayed similar results in PANC-1 cells. All monometallic complexes, except for **Pd-3**, reduced cell viability by more than 50% in PANC-1 cells. Also worth mentioning is that all heterobimetallic complexes outperformed cisplatin in RH30 cells, with only **PdRu-2** and **PdOs-2** reducing cell viability by less than 50%, albeit by a narrow margin (51.86% and 52.65%,

Table 1 Summary of percentage (%) cell viability of various cancer cell lines after 48 h 10 μM treatment with complexes

Cell line Complex	Cervical cancer		Pancreatic cancer		Rhabdomyosarcoma		Breast cancer		Non-malignant
	HeLa	Ca Ski	PANC-1	CFPAC-1	RD	RH30	MCF-7	MDA-MB-231	MRC-5
DMSO	100.00 ± 4.27	100.00 ± 1.95	100.00 ± 11.69	100.00 ± 7.11	100.00 ± 0.00	100.00 ± 0.00	100.00 ± 1.09	100.00 ± 5.19	100.00 ± 0.00
PtPt-0	95.48 ± 6.36	86.35 ± 2.35	85.44 ± 5.42	82.06 ± 6.94	87.70 ± 7.54	106.80 ± 7.54	96.93 ± 2.20	104.13 ± 3.69	—
Pd-1	63.35 ± 2.64	77.78 ± 1.48	**32.10 ± 3.54**	76.13 ± 5.23	75.43 ± 5.55	62.63 ± 6.48	73.22 ± 1.79	85.34 ± 7.91	—
Pd-2	89.11 ± 2.45	96.02 ± 5.51	**41.02 ± 6.99**	100.98 ± 9.34	63.78 ± 2.66	82.62 ± 2.15	85.08 ± 1.67	85.80 ± 4.49	—
Pd-3	87.13 ± 1.38	97.92 ± 0.10	67.32 ± 7.50	91.70 ± 4.49	89.00 ± 0.37	86.44 ± 7.67	85.63 ± 0.21	93.45 ± 2.65	—
Pt-1	84.58 ± 0.75	88.85 ± 0.69	**45.85 ± 7.87**	64.94 ± 4.09	74.87 ± 9.61	82.06 ± 1.38	85.58 ± 0.84	93.95 ± 7.53	—
Pt-2	90.00 ± 1.66	88.57 ± 2.48	**34.18 ± 7.20**	83.07 ± 4.48	62.76 ± 1.54	74.35 ± 3.60	86.81 ± 1.49	76.15 ± 4.44	—
Pt-3	86.05 ± 4.10	69.74 ± 1.78	**34.89 ± 14.92**	66.07 ± 6.01	76.20 ± 8.00	78.57 ± 2.64	72.61 ± 0.65	94.08 ± 3.06	—
PdRu-1	**37.41 ± 1.44**	**26.58 ± 7.22**	**9.41 ± 2.86**	**25.42 ± 5.68**	51.17 ± 1.57	**34.29 ± 2.80**	**28.39 ± 3.50**	**45.19 ± 4.45**	50.63 ± 8.37
PdRu-2	61.79 ± 3.91	**43.49 ± 2.67**	**16.19 ± 2.59**	**21.53 ± 3.69**	67.77 ± 9.41	51.86 ± 8.26	65.34 ± 0.40	92.41 ± 4.58	76.38 ± 11.17
PdRu-3	62.19 ± 4.97	**34.07 ± 1.29**	**28.11 ± 3.95**	**30.50 ± 7.74**	70.73 ± 0.82	**42.23 ± 4.21**	75.31 ± 0.03	73.33 ± 8.70	72.64 ± 2.52
PtRu-1	**46.19 ± 3.39**	**31.80 ± 2.41**	**12.97 ± 13.15**	**24.90 ± 2.64**	81.63 ± 3.40	**45.37 ± 1.89**	84.73 ± 0.70	104.11 ± 5.64	66.22 ± 8.14
PtRu-2	65.46 ± 3.25	**40.07 ± 1.55**	**14.77 ± 8.18**	**17.88 ± 4.20**	66.24 ± 12.99	**46.20 ± 6.39**	78.68 ± 1.96	64.57 ± 6.86	84.42 ± 19.53
PtRu-3	59.51 ± 3.61	**30.57 ± 2.72**	**22.68 ± 11.69**	**13.93 ± 5.16**	76.65 ± 5.55	**48.07 ± 2.05**	73.43 ± 0.78	**48.47 ± 6.06**	79.74 ± 13.03
PdOs-1	58.49 ± 1.89	**32.63 ± 2.29**	**21.55 ± 1.81**	33.56 ± 4.88	58.93 ± 0.49	**32.12 ± 9.76**	63.78 ± 1.82	83.66 ± 3.20	68.44 ± 9.17
PdOs-2	74.27 ± 0.87	**37.55 ± 1.29**	**18.29 ± 3.36**	37.70 ± 4.42	72.66 ± 0.62	52.65 ± 7.30	75.29 ± 1.76	**44.52 ± 2.51**	71.27 ± 7.57
PdOs-3	**36.08 ± 3.46**	**26.67 ± 2.94**	**23.33 ± 3.71**	**33.48 ± 3.89**	64.17 ± 2.46	**47.94 ± 8.70**	51.79 ± 5.18	55.33 ± 10.39	69.80 ± 1.02
PdPd-1	89.05 ± 4.85	69.67 ± 4.89	**31.36 ± 5.31**	64.17 ± 5.82	79.21 ± 3.45	**44.05 ± 12.45**	80.69 ± 7.24	82.58 ± 9.21	—
PdPd-2	68.55 ± 4.35	57.25 ± 4.35	**19.42 ± 4.48**	84.58 ± 10.91	54.80 ± 4.71	**39.25 ± 12.57**	89.21 ± 13.53	115.61 ± 5.53	—
PdPd-3	72.96 ± 6.31	62.28 ± 0.64	64.16 ± 14.09	82.09 ± 9.04	94.67 ± 3.95	87.13 ± 17.73	95.63 ± 2.71	98.08 ± 11.43	—
Cisplatin	70.41 ± 5.81	**31.33 ± 2.65**	**31.57 ± 3.02**	**43.59 ± 4.18**	79.54 ± 0.56	65.85 ± 21.80	81.42 ± 2.03	86.30 ± 2.20	74.23 ± 6.74

The complexes that reduced % cell viability by more than 50% are highlighted in bold, and the complexes outperforming cisplatin are highlighted in red.

respectively). Regarding the Ca Ski cell line, all heterobimetallic complexes reduced cell viability by more than 50%, with **PdRu-1**, **PtRu-3** and **PdOs-3** outperforming cisplatin. On HeLa cells, three complexes (**PdRu-1**, **PtRu-1** and **PdOs-3**) reduced cell viability by more than 50%, whereas all heterobimetallic complexes except **PdOs-2** outperformed cisplatin, as well as **Pd-1** and **PdPd-2**. Most of the complexes tested outperformed cisplatin in RD cells. However, none reduced cell viability by more than 50%. In MCF-7 cells, only **PdRu-1** reduced cell viability by more than 50%, whereas all heterobimetallic complexes, except **PtRu-1**, as well as **Pd-1**, **Pt-3** and **PdPd-1**, outperformed cisplatin. Finally, in MDA-MB-231 cells, the heterobimetallic complexes generally perform better, with **PdRu-1**, **PtRu-3** and **PdOs-2** reducing cell viability by more than 50% and outperforming cisplatin. None of the complexes tested at 10 μM inhibited non-malignant MRC-5 cell viability by more than 50%, and none were more cytotoxic than cisplatin, which indicates the potential for selectivity in this molecular design.

PdRu-1 and **PdOs-3** were determined to be the best-performing complexes overall through averaging of the percentage cell viability values obtained over the eight cancer cell lines. These two complexes were therefore further investigated in cervical and pancreatic cell lines because they were most cytotoxic in those, while displaying minimal cytotoxicity against the non-malignant cell line. The IC_{50} values were determined by multidose experiments in the cervical cancer and pancreatic cancer cell lines as well as in the non-malignant FG0 cell line. The related selectivity indices were derived by dividing the IC_{50} values in the non-malignant cells by the IC_{50} values in the cancer cells (Table 2 and Fig. S184–S186). Both complexes outperformed cisplatin in the four cell lines tested.[63,64] In the cervical cancer cells, **PdRu-1** showed high selectivity (SI ≥ 5) for Ca Ski cells and moderate selectivity (2 ≤ SI ≤ 5) for HeLa cells, whereas **PdOs-3** showed moderate selectivity for Ca Ski cells only. In pancreatic cancer cell lines, both **PdRu-1** and **PdOs-3** displayed moderate selectivity for PANC-1 cells but low selectivity (SI ≤ 2) towards CFPAC-1 cells.

Surprisingly, a correlation could not be drawn between diphosphine spacer length and biological activity, which contrasts with our previous report on some heterobimetallic Fe–Ru(II) complexes.[38] However, a clear trend can be observed in terms of activity of the different types of complexes reported herein: the heterobimetallic complexes perform better than their homo- and monometallic counterparts across all cancer cell lines tested, apart from few exceptions. Apart from CFPAC-1, where the Os-based heterobimetallic complexes seemed somewhat less active than the Ru-containing complexes, having Ru(II) or Os(II) does not seem to greatly affect activity. In Ca Ski and RH30, the homobimetallic complexes generally outperform the monometallic complexes. In the other cell lines, activities are roughly comparable. Details on the cell-lines: PANC-1 (ATCC; CRL-1469), CFPAC-1 (ATCC; CRL-1918), MRC-5 (ATCC; CCL-171), HeLa (ATCC; CCL-2), Ca Ski (ATCC; CRL-1550); RD (ATCC; CCL-136TM), MCF-7 (ATCC; HTB-22TM), MDA-MB-231 (ATCC; HTB-26TM).

Table 2 IC$_{50}$ values (μM) determined for the most active complexes, **PdRu-1** and **PdOs-3**, in cervical, pancreatic and non-malignant cell lines

| Complex | | Cervical cancer | | Pancreatic cancer | | Non-malignant FG0 |
		HeLa	Ca-Ski	PANC-1	CFPAC-1	
PdRu-1	IC$_{50}$	6.87 ± 0.97	3.43 ± 1.32	5.69 ± 1.87	17.56 ± 1.14	21.12 ± 1.75
	SI	3.07	6.16	3.71	1.20	—
PdOs-3	IC$_{50}$	23.84 ± 2.59	12.05 ± 1.99	12.53 ± 1.61	28.07 ± 1.08	30.41 ± 2.09
	SI	1.28	2.52	2.43	1.08	—
Cisplatin	IC$_{50}$	66.03 (ref. 63)	17.46 (ref. 63)	87.86 ± 2.29 (ref. 64)	41.31 (ref. 63)	—

Selectivity indices (SI) derived by the following equation: IC$_{50}$ FG0 cells/IC$_{50}$ cancer cells, where SI ≤ 2: low selectivity, 2 ≤ SI ≤ 5: moderate selectivity, and SI ≥ 5: high selectivity.

Aquation studies

Aquation studies were conducted using UV-Vis spectroscopy on one example complex per homologous series at $C = 5 \times 10^{-6}$ M in a PBS buffer : DMSO solution (90 : 10 v/v) in order to identify the potential species forming in biological media. All the kinetic plots can be found in the SI (Fig. S187–S192). In the case of monometallic complex **Pd-2**, biphasic spectral changes are observed, which fit a double-exponential decay function, indicating two processes occurring one after the other. The first process ($k_1 = 2.38 \times 10^{-2}$ min^{-1}) is tentatively attributed to hydrolysis at the Pd(II) centre, followed by HCl elimination ($k_2 = 2.58 \times 10^{-6}$ min^{-1}) to form a hydroxo complex. Phosphane dissociation, to account for the second process can be entirely ruled out, as NMR experiments performed over this time period did not show any phosphane dissociation. Similar results were observed in the case of **Pt-2**, even though the rates are comparatively, faster than **Pd-2**. The initial ligand exchange rate is in the same order of magnitude

($k_1 = 7.15 \times 10^{-2}$ min^{-1}), which comes as a surprise, owing to Pd's typically faster ligand exchange kinetics.[65] HCl elimination is seemingly much faster in **Pt-2** ($k_2 = 1.15 \times 10^{-2}$ min^{-1}) compared to **Pd-2**. Regarding **PdPd-3**, a single exponential decay ($k_1 = 2.13 \times 10^{-3}$ min^{-1}) is observed on the time scale of the experiment (Fig. 7). This likely indicates either one of two things: a. aquation step occurs at one of the Pd(II) centers, generating a monoaqua complex bearing a +3 charge and a Cl counteranion, or b. aquation occurs, followed by fast HCl elimination (faster than the experimental time scale) in order to restore the more stable +2 charged complex. The rate of aquation is somewhat similar to k_1 in **Pd-2**, which supports aquation at Pd(II) as the first/sole step in **PdPd-3**. Concerning the heterobimetallic complexes, the speciation is more complicated. Regarding **PdRu-2**, a two steps process with first a decrease in absorbance ($k_1 = 4.46 \times 10^{-2}$ min^{-1}), followed by an increase ($k_2 = 9.17 \times 10^{-2}$ min^{-1}) is observed. However, **PtRu-2** follows exclusively a double exponential decay indicating also a two-step mechanism ($k_1 = 2.97 \times 10^{-1}$ min^{-1} and k_2
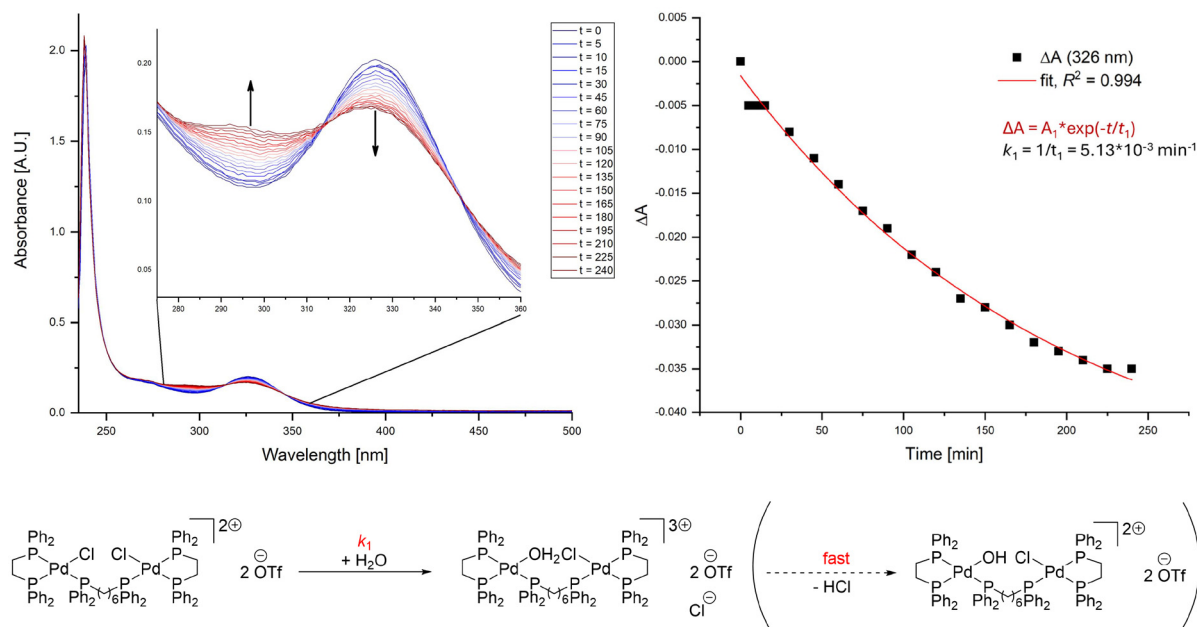
Fig. 7 UV-Vis spectral changes over time of **PdPd-3** ($C = 5 \times 10^{-6}$ M) in a 90 : 10 PBS buffer (pH = 7.45) : DMSO solution at 37 °C (top left), plot of the change in absorbance over time at 326 nm (top right), and hypothesised mechanism (bottom).
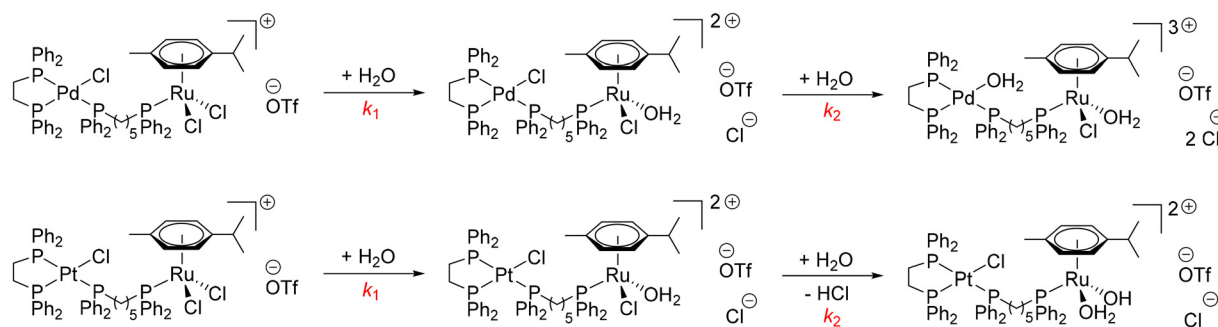
Scheme 8 Putative product formation upon hydrolysis of **PdRu-2** (top) and **PtRu-2** (bottom) in biological media.

$= 2.71 \times 10^{-2}$ min^{-1}). Finally, **PdOs-2** undergoes a three steps process, with first a single exponential increase in absorbance ($k_1 = 2.88 \times 10^{-1}$ min^{-1}), followed by a double exponential decay ($k_2 = 2.52 \times 10^{-2}$ min^{-1} and $k_3 = 3.57 \times 10^{-2}$ min^{-1}). We tentatively assign hydrolysis at Ru(II), followed by a second hydrolysis at Ru(II) and HCl elimination in the case of **PtRu-2** to afford an Ru(II) aqua hydroxo complex as with previous findings reported by us (Scheme 8, bottom).[38] In the case of **PdRu-2**, the decrease in absorbance indicates likely hydrolysis at Ru(II), while the increase in absorbance is indicative of hydrolysis occurring at Pd(II), as is also observed in **PdOs-2**. It is hence the case in **PdOs-2**, that hydrolysis occurs first at Pd(II), which would explain the increase in absorbance observed. Hydrolysis at Os(II) happens afterwards due to Os increased inertness. The third process can either be HCl elimination to form a Pd-hydroxo complex, or else hydrolysis followed by HCl elimination at Os(II), in a similar fashion as **PtRu-2**.

A tentative link to activity *in vitro* can be derived from the above speciation experiments. Indeed, the mononuclear complexes were determined to be rather inactive *in vitro*, which is consistent with the formation of a more biologically inert hydroxo complex. The homodinuclear complexes showed slightly higher biological activity than their mononuclear counterparts, which can be attributed to one Pd(II) still bearing a labile Cl co-ligand which can later be substituted for binding to a suitable biological target, as is the case with the mechanism of cisplatin.[66] Regarding the heterobimetallic complexes, the PtRu series showed slightly less activity than the Pd-based examples, which might be due to a more inert Pt(II) center, whereas a labile OH$_2$ bound to Ru(II) is present. Regarding the PdOs series, in both possible species a labile OH$_2$ is present at Os(II), whereas in the case of Pd, either a Pd-hydroxo or Pd-aqua complex is possible, Pd-aqua likely being more active. Finally, the PdRu series was determined to be the most active of all, which is consistent with the formation of a doubly aquated complex, with labile OH$_2$ groups on both Pd(II) and Ru(II) (Scheme 8, top).

Conclusions

Mononuclear Pd(II) and Pt(II)-based complexes, bearing pendant diphosphines, their corresponding homodinuclear Pd–Pd, and heterodinuclear Pd(II)–Ru(II), Pt(II)–Ru(II) and Pd(II)–Os(II) complexes bearing bridging diphosphines have been reported and fully characterised by spectroscopic means. Their *in vitro* cytotoxic activity was determined on eight cancerous cell lines and a non-malignant cell line, as well as IC$_{50}$ values and selectivity indices of the most active complexes in the series. No obvious relationship between the diphosphine tether or spacer length and activity could be derived, although a strong correlation between the heterobimetallic nature of the complexes and higher biological activity was observed, possibly due to the different species formed upon aquation in biological media, as demonstrated by our tentative aquation studies. The monometallic and homobimetallic complexes displayed suboptimal activities *in vitro*, which suggests the need for hetero metals in future bimetallic anticancer drug designs for complexes containing Pd(II) and Pt(II). The complexes reported herein highlight a novel class of compounds which encourages the pursuit of heterobimetallic scaffolds as an enhanced molecular design for the next generation of anticancer drugs.

Experimental section

General considerations

The chemicals were handled using standard Schlenk techniques, unless otherwise stated. Solvents used were dried and degassed using standard techniques prior to use. [(κ^2-dppe)PdCl$_2$] (TCI), AgOTf (Sigma-Aldrich), 1,4-bis(diphenylphosphino)butane (dppb) (Sigma-Aldrich), 1,5-bis(diphenylphosphino)pentane (dpppent) (Sigma-Aldrich), 1,6-bis(diphenylphosphino)hexane (dpph) (Sigma-Aldrich), [(*p*-cym)RuCl$_2$]$_2$ (Strem), [(COD)PtCl$_2$] (Strem), were used as received. EtOH (100%), acetonitrile, dichloromethane (stab. amylene), THF, Et$_2$O were purchased from Biosolve. DMSO-d_6, CDCl$_3$ and acetone-d_6 were purchased from VWR chemicals. [(*p*-cym)OsCl$_2$]$_2$ and [(κ^2-dppe)PdCl$_2$] were synthesised according to literature proceedings.[48,67] NMR spectra were recorded on a JEOL JNM-ECZ400s FT NMR spectrometer. NMR data was processed using MestReNova v14.3.0, and reported in parts per million (ppm) referenced to TMS (^{1}H and ^{13}C{^{1}H}), 85% phosphoric acid (^{31}P{^{1}H}) or CFCl$_3$ (^{19}F{^{1}H}). The peak multiplici-

ties abbreviations are as follows: s = singlet, d = doublet, t = triplet, q = quartet, sept = septet, m = multiplet, ps = pseudo, br = broad. FT-IR spectra were recorded on a Shimadzu IRSpirit FTIR spectrometer, using the following parameters: 64 scans, resolution 4, Happ-Genzel apodization, with a scan range of 4000–400 cm^{-1}. The signals reported as follows: s = strong, m = medium, w = weak, v = very, br = broad. UV-Vis absorption spectra were recorded using 1 cm pathlength quartz cuvettes on a Shimadzu UV-3600 iPlus-1 spectrometer within a range of 190–800 nm. OriginPro 2018 SR1 b9.5.1.195 was used for data processing of IR and UV-Vis data. Mass spectrometry was conducted using a Waters Syanpt G2S ESI-TOF-MS (3 kV) and the spectra processed using MassLynx™ v4.2 and the experimentally determined spectra accuracy and isotope patterns were checked using the built-in isotope calculator. Melting points were obtained on a Stuart SMP10 Digital Melting Point apparatus, performed in duplicate and the average reported in °C. Single crystal X-ray diffraction analysis was performed on a Rigaku XtaLAB Synergy, Dualflex, HyPix-Arc 100 diffractometer using Cu radiation (λ = 1.54184 Å). CrysAlisPro was used to reduce data to F_o^2 and corrected for absorption effects. Structures were solved using SHELXT and refined with SHELXL as implemented in OLEX2.

Synthesis of [(κ²-dppe)PdCl]$_2$(2OTf) (PdPd-0). 2.05 g (3.56 mmol, 1.00 eq.) of [(κ²-dppe)PdCl$_2$] were dissolved in dichloromethane (35 mL). 0.914 g (3.56 mmol, 1.00 eq.) of AgOTf was added to the solution while stirring at room temperature. The reaction vessel was covered in aluminium foil and the mixture was left to stir at room temperature for 1 hour. The resulting solution was filtered through a Schlenk-frit, and the filtrate evaporated and dried *in vacuo*. Properties: reverts to [(κ²-dppe)PdCl$_2$] in chloroform, forms [(κ²-dppe)PdCl(DMSO)] (OTf) in dimethyl sulfoxide, insoluble in tetrahydrofuran and soluble in acetone. 1.99 g (81%) of bright yellow solid, air stable. ^{1}H NMR (400.130 MHz, acetone-d_6, 298 K): δ 7.91–7.81 (16H, m, P*Ph*), 7.77–7.70 (8H, m, P*Ph*), 7.65–7.57 (16H, m, P*Ph*), 3.14 (8H, ps d, C*H*$_2$, κ²-dppe). ^{13}C{^{1}H} NMR (100.613 MHz, acetone-d_6, 298 K): δ 134.6–134.3 (m, P*Ph*), 130.8–130.4 (m, P*Ph*), 28.2 (ps d, C*H*$_2$, κ²-dppe). ^{31}P{^{1}H} NMR (161.976 MHz, acetone-d_6, 298 K): δ 76.9 (br s, $\Delta\nu_{1/2}$ = 158.7 Hz, P*Ph*$_2$). ^{31}P{^{1}H} NMR (161.976 MHz, DMSO-d_6, 298 K): δ 70.9 (br ps d, $\Delta\nu_{1/2}$ = 60.0 Hz, P^A), 69.0 (br ps d, $\Delta\nu_{1/2}$ = 60.8 Hz, $^2J_{\text{P}^B-\text{P}^A}$ = 11.5 Hz, P^B). ^{19}F NMR (376.498 MHz, DMSO-d_6, 298 K): δ −77.6 (OTf). FT-IR (cm^{-1}): 3058 (vw), 2963 (vw), 1436 (m), 1256 (br s), 1223 (m), 1148 (m), 1099 (m), 1027 (s), 997 (w), 815 (m), 707 (m), 687 (s), 635 (vs), 527 (vs), 480 (m). UV/Vis $\lambda_{\max}$ (dichloromethane): 227 nm (major, ε = 120 952 M^{-1} cm^{-1}), 276 nm (ε = 60 533 M^{-1} cm^{-1}), 346 (minor, ε = 27 924 M^{-1} cm^{-1}). ESI-TOF-MS (3 kV, dichloromethane): m/z calcd for [M-OTf]$^+$, 1229.0; expt., 1228.9. m/z calcd for [M-2OTf + Cl]$^+$, 1115.0; expt., 1114.9. m/z calcd for [(κ²-dppe)Pd(OTf)]$^+$, 653.0; expt., 653.0. m/z calcd for [(κ²-dppe)PdCl]$^+$, 541.0; expt., 541.0 (100%).

Synthesis of [(κ²-dppe)PtCl]$_2$(2OTf) (PtPt-0). 450 mg of [Pt (κ²-dppe)Cl$_2$] (0.677 mmol, 1.00 eq.) and 174 mg of AgOTf (0.677 mmol, 1.00 eq.) were added as solids in a Schlenk tube,

and dissolved in 50 mL of dichloromethane. The solution was stirred in the dark for 1.5 h at room temperature, and subsequently filtered, washed with Et$_2$O and dried *in vacuo*. 381 mg (70%) of white powder, air stable. Melting point: progressive browning from 160 °C to 180 °C. ^{1}H NMR (400.130 MHz, DMSO-d_6, 293 K): δ 7.94–7.55 (40 H, m, P*Ph*), 2.73 (8 H, m, 4 × C*H*$_2$, κ²-dppe). ^{1}H NMR (400.130 MHz, acetone-d_6, 293 K): δ 8.48–7.14 (40 H, unresolved m, P*Ph*), 3.06 (8 H, br s, κ²-dppe). ^{13}C{^{1}H}NMR (100.613 MHz, DMSO-d_6, 293 K): δ 133.7 (unresolved m, P*Ph*), 132.7 (dd, $^xJ_{\text{C-P}}$ = 17.95 Hz, $^xJ_{\text{C-P}}$ = 2.71 Hz, P*Ph*), 129.8–129.6 (unresolved m, P*Ph*), 129.3 (dd, $^xJ_{\text{C-P}}$ = 26.64 Hz, $^xJ_{\text{C-P}}$ = 11.60 Hz, P*Ph*), 126.1 (d, $^xJ_{\text{C-P}}$ = 66.71 Hz, P*Ph*), 125.9 (d, $^xJ_{\text{C-P}}$ = 64.45 Hz, P*Ph*), 120.7 (d, $^xJ_{\text{C-P}}$ = 322.79 Hz, P*Ph*), 27.4 (ps s, κ²-dppe). ^{31}P{^{1}H} NMR (161.976 MHz, DMSO-d_6, 293 K): δ 45.9 (br s, $^1J_{\text{P-Pt}}$ = 3636 Hz, $\Delta\nu_{1/2}$ = 66.3 Hz). ^{31}P{^{1}H} NMR (161.976 MHz, acetone-d_6, 293 K): δ 49.0 (s, $^1J_{\text{P-Pt}}$ = 3780.8 Hz). ^{19}F NMR (376.498 MHz, DMSO-d_6, 293 K): δ −77.7 (s, OTf). FT-IR (cm^{-1}): 3057 (w), 2963 (w), 2922 (w), 1438 (m), 1258 (s), 1224 (m), 1143 (m), 1104 (s), 1027 (s), 798 (s), 720 (s), 708 (s), 688 (s), 635 (s), 532 (s), 517 (s), 480 (s). UV/Vis $\lambda_{\max}$ (dichloromethane): 226 nm (major, ε = 55 924 M^{-1} cm^{-1}), 302 nm (minor, ε = 3676 M^{-1} cm^{-1}). ESI-TOF-MS (3 kV, dichloromethane): m/z calcd for [(κ²dppe) PtCl]$_2$Cl$^+$, 1293.1; expt., 1293.1 (<1%); m/z calcd for [(κ²dppe) PtCl]$^+$, 629.1; expt., 629.1 (100%).

General procedure for the synthesis of [(κ²-dppe)PdCl(κ¹-dppx)](OTf) (Pd-*x*)

200 mg (0.145 mmol, 1.00 eq.) of **PdPd-0** were dissolved in dichloromethane (5 mL). Separately, the respective diphosphine (0.29 mmol, 2.00 eq.) was dissolved in dichloromethane (5 mL) in a Schlenk flask. The solution of **PdPd-0** was added dropwise to the diphosphine solution and the resulting solution was stirred at room temperature for one hour. The solvent was removed *in vacuo*, after which the resulting solid was washed with diethyl ether (10 mL). The product was subsequently dried *in vacuo* overnight. (In the case of **Pd-3**, 142 mg (0.103 mmol, 1.00 eq.) of **PdPd-0** were used in the synthesis).

Characterisation of [(κ²-dppe)PdCl(κ¹-dppb)](OTf) (Pd-1)

235 mg (72%) of pale yellow solid, air stable. Melting point: 125–130 °C (melt), 150 °C + (dec.). ^{1}H NMR (400.130 MHz, DMSO-d_6, 298 K): δ 7.90–7.10 (40H, m, P*Ph*), 2.85 (2H, br d, $^2J_{\text{H-P}}$ = 35 Hz, PC*H*$_2$^{A}C*H*$_2$^{B}P, κ²-dppe), 2.46 (obscured by solvent, 2H, br d, PC*H*$_2$^{A}C*H*$_2$^{B}P, κ²-dppe), 2.18 (2H, br s, $\Delta\nu_{1/2}$ = 27.3 Hz, 1 × C*H*$_2$, dppb), 2.10–1.80 (2H, br m, 1 × C*H*$_2$, dppb), 1.47 (2H, br s, $\Delta\nu_{1/2}$ = 27.1 Hz, 1 × C*H*$_2$, dppb), 1.27 (2H, br s, $\Delta\nu_{1/2}$ = 27.7 Hz, 1 × C*H*$_2$, dppb). ^{13}C{^{1}H} NMR (100.613 MHz, DMSO-d_6, 298 K, aliphatic signals not visible, assigned from ^{1}H–^{13}C 2D HSQC spectrum): δ 134.3–128.9 (unresolved m, P*Ph*), 33.2 (PC^A*H*$_2$C^B*H*$_2$P, κ²-dppe), 26.8 (1 × C*H*$_2$, dppb), 26.6 (1 × C*H*$_2$, dppb), 26.5 (1 × C*H*$_2$, dppb), 25.1 (1 × C*H*$_2$, dppb), 24.1 (PC^A*H*$_2$C^B*H*$_2$P, κ²-dppe). ^{31}P{^{1}H} NMR (161.976 MHz, DMSO-d_6, 298 K): δ 65.5–66.4 (br d, P^B, conformer A + B), 64.8 (dd, $^2J_{\text{P}^A-\text{P}^C}$ = 411 Hz, $^2J_{\text{P}^A-\text{P}^B}$ = 7.3 Hz, P^A, conformer A + B), 18.1 (dd, $^2J_{\text{P}^C-\text{P}^A}$ = 411.2 Hz, $^2J_{\text{P}^C-\text{P}^B}$ = 17.5 Hz, P^C, conformer B), 17.8

(dd, $^2J_{\text{PC–PA}}$ = 410.2 Hz, $^2J_{\text{PC–PB}}$ = 17.9 Hz, P^C, conformer A), −15.9 (br s, $\Delta\nu_{1/2}$ = 205 Hz, P^D, conformer B), −17.2 (br s, $\Delta\nu_{1/2}$ = 32.5 Hz, P^D, conformer A). ^{19}F NMR (376.498 MHz, DMSO-d_6, 298 K): δ −77.6 (OTf). FT-IR (cm^{-1}): 3055 (vw), 2933 (vw), 1436 (m), 1262 (vs), 1223 (m), 1147 (m), 1101 (m), 1029 (s), 999 (m), 741 (m), 690 (vs), 635 (vs), 530 (s), 516 (s), 480 (s). UV/Vis λ_{max} (dichloromethane): 227 (major), 267 (shoulder), 331 (minor). ESI-TOF-MS (3 kV, dichloromethane): m/z calcd for [(κ^2-dppe)PdCl(κ^1-dppb)]$^+$, 965.2; expt., 965.4 (100%). m/z calcd for [(κ^2-dppe)PdCl]$^+$, 541.0; expt., 541.1 (7%).

Characterisation of [(κ^2-dppe)PdCl(κ^1-dpppent)](OTf) (Pd-2)

216 mg (76%) of pale-yellow solid, air stable. ^{1}H NMR (400.130 MHz, DMSO-d_6, 298 K): δ 7.85–7.14 (40 H, unresolved m, P*Ph*), 2.84 (2 H, br d, $^2J_{\text{H–P}}$ = 34.9 Hz, PCH_2^ACH_2^BP, κ^2-dppe), 2.47 (obscured by solvent) (2 H, obscured br d, PCH_2^ACH_2^BP, κ^2-dppe), 2.34–2.16 (2 H, br s, $\Delta\nu_{1/2}$ = 27.8 Hz, 1 × CH_2, dpppent), 2.03–1.88 (2 H, br m, $\Delta\nu_{1/2}$ = 28.6 Hz 1 × CH_2, dpppent), 1.55–1.26 (4 H, m, 2 × CH_2, dpppent), 1.26–1.13 (2 H, br s, $\Delta\nu_{1/2}$ = 24.4 Hz, 1 × CH_2, dpppent). ^{13}C{^{1}H} NMR (signals assigned from HSQC spectrum) (100.613 MHz, DMSO-d_6, 298 K): δ 128.9–134.3 (unresolved m, P*Ph*), 33.3 (s, PCH_2^ACH_2^BP, κ^2-dppe), 31.9 (1 × CH_2, dppp), 31.8 (1 × CH_2, dppp), 26.5 (1 × CH_2, dppp), 25.3 (1 × CH_2, dppp), 25.2 (1 × CH_2, dppp), 24.3 (1 × Ph$_2$PC^{A}H$_2$C^{B}H$_2$PPh$_2$). ^{31}P{^{1}H} NMR (161.976 MHz, DMSO-d_6, 298 K): δ 66.5–66.1 (br m, $\Delta\nu_{1/2}$ = 36.5 Hz, P^B, conformer A + B), 64.7 (dd, $^2J_{\text{PA–PC}}$ = 411.9 Hz, $^2J_{\text{PA–PB}}$ = 6.8 Hz, P^A, conformer B), 64.6 (dd, $^2J_{\text{PA–PC}}$ = 411.1 Hz, $^2J_{\text{PA–PB}}$ = 5.1 Hz, P^A, conformer A), 18.1 (dd, $^2J_{\text{PC–PA}}$ = 411.8 Hz, $^2J_{\text{PC–PB}}$ = 19.7 Hz, P^C, conformer B), 17.8 (dd, $^2J_{\text{PC–PA}}$ = 408.6 Hz, $^2J_{\text{PC–PB}}$ = 19.5 Hz, P^C, conformer A), −16.1 (br s, (in baseline), P^D, conformer B), −16.9 (br s, $\Delta\nu_{1/2}$ = 16.6 Hz, P^D, conformer A). ^{19}F NMR (376.498 MHz, DMSO-d_6, 298 K): δ −77.6 (OTf). FT-IR (cm^{-1}): 3054 (vw), 2926 (vw), 2855 (vw), 1434 (m), 1262 (s), 1221 (w), 1147 (m), 1099 (m), 1030 (s), 999 (w), 741 (m), 690 (vs), 635 (vs), 530 (s), 514 (s), 481 (s). UV/Vis λ_{max} (dichloromethane): 227 (major), 261 (shoulder), 332 (minor). ESI-TOF-MS (3 kV, dichloromethane): m/z calcd for [(κ^1-dppe)PdCl(κ^1dppp)]$^+$, 979.2; expt., 979.3 (100%). m/z calcd for [(κ^2-dppe)PdCl]$^+$, 541.0; expt., 541.1 (24%). Temperature studies: ^{1}H NMR (400.130 MHz, DMSO-d_6, 343 K): δ 7.91–7.09 (40 H, unresolved m, P*Ph*), 2.82 (2 H, br d, $^2J_{\text{H–P}}$ = 33.3 Hz, PCH_2^ACH_2^BP, κ^2-dppe), 2.46 (obscured by solvent) (2 H, obscured br d, PCH_2^ACH_2^BP, κ^2-dppe), 2.34–1.85 (4 H, ps m, 2 × CH_2, dpppent, pseudo coalescent signals), 1.53–1.15 (6 H, ps br s, $\Delta\nu_{1/2}$ = 55.1 Hz, 3 × CH_2, dpppent, coalescent signals). ^{1}H NMR (400.130 MHz, DMSO-d_6, 353 K): δ 7.91–7.12 (40 H, unresolved m, P*Ph*), 2.82 (2 H, br d, $^2J_{\text{H–P}}$ = 32.5 Hz, PCH_2^ACH_2^BP, κ^2-dppe), 2.45 (obscured by solvent) (2 H, obscured br d, PCH_2^ACH_2^BP, κ^2-dppe), 2.30–1.90 (4 H, ps m, 2 × CH_2, dpppent, pseudo coalescent signals), 1.53–1.15 (6 H, br s, $\Delta\nu_{1/2}$ = 55.8 Hz, 3 × CH_2, dpppent, coalescent signals). ^{31}P{^{1}H} NMR (161.976 MHz, DMSO-d_6, 343 K): δ 66.0 (br s, $\Delta\nu_{1/2}$ = 30.8 Hz, P^B, coalescent signals), 64.7 (ps dd, $^2J_{\text{PA–PC}}$ = 412.0 Hz, P^A, coalescent signals), 18.2 (ps d, $^2J_{\text{PC–PA}}$ = 416.0 Hz, P^C, coalescent signals), −14.8 (m, P^D, conformer B) −15.5 (br s, $\Delta\nu_{1/2}$ = 72.4 Hz,

P^D, conformer A). ^{31}P{^{1}H} NMR (161.976 MHz, DMSO-d_6, 353 K): δ 66.0 (br s, $\Delta\nu_{1/2}$ = 30.1 Hz, P^B, coalescent signals), 64.8 (ps dd, $^2J_{\text{PA–PC}}$ = 406.8 Hz, P^A, coalescent signals), 18.2 (ps d, $^2J_{\text{PC–PA}}$ = 411.9 Hz, P^C, coalescent signals), −14.2 (m, in baseline, P^D, conformer B), −15.3 (br s, $\Delta\nu_{1/2}$ = 64.4 Hz, P^D, conformer A).

Characterisation of [(κ^2-dppe)PdCl(κ^1-dpph)](OTf) (Pd-3)

159 mg (77%) of pale-yellow solid, air stable. ^{1}H NMR (400.130 MHz, DMSO-d_6, 298 K): δ 7.91–7.10 (40 H, unresolved m, P*Ph*), 2.84 (2 H, br d, $^2J_{\text{H–P}}$ = 34.7 Hz, PCH_2^ACH_2^BP, κ^2-dppe), 2.44 (obscured by solvent) (2 H, obscured br d, PCH_2^ACH_2^BP, κ^2-dppe), 2.29 (2 H, br s, $\Delta\nu_{1/2}$ = 27.4 Hz, 1 × CH_2, dpph), 2.01 (2 H, br s, $\Delta\nu_{1/2}$ = 21.8 Hz, 1 × CH_2, dpph), 1.40–1.00 (8 H, unresolved m, 4 × CH_2, dpph). ^{13}C{^{1}H} NMR (signals assigned from HSQC spectrum) (100.613 MHz, DMSO-d_6, 298 K): δ 134.3–128.9 (unresolved m, P*Ph*), 33.2 (PCH_2^ACH_2^BP, κ^2-dppe), 30.6 (1 × CH_2, dpph), 30.3 (1 × CH_2, dpph), 30.1 (1 × CH_2, dpph), 26.7 (1 × CH_2, dpph), 25.6 (1 × CH_2, dpph), 25.3 (1 × CH_2, dpph), 24.3 (PCH_2^ACH_2^BP, κ^2-dppe). ^{31}P{^{1}H} NMR (161.976 MHz, DMSO-d_6, 298 K): δ 66.5–66.1 (br d, $\Delta\nu_{1/2}$ = 38.3 Hz, P^B, conformer A + B), 64.7 (dd, $^2J_{\text{PA–PC}}$ = 415 Hz, $^2J_{\text{PA–PB}}$ = 5 Hz, P^A, conformer B), 64.6 (dd, $^2J_{\text{PA–PC}}$ = 411.2 Hz, $^2J_{\text{PA–PB}}$ = 5.4 Hz, P^A, conformer A), 18.0 (dd, $^2J_{\text{PC–PA}}$ = 410.7 Hz, $^2J_{\text{PC–PB}}$ = 19.5 Hz, P^C, conformer B), 17.6 (dd, in baseline, P^C, conformer A), −16.5 (br s, in baseline P^D, conformer B), −16.9 (br s, $\Delta\nu_{1/2}$ = 16.6 Hz, P^D, conformer A). ^{19}F NMR (376.498 MHz, DMSO-d_6, 298 K): δ −77.6 (OTf). FT-IR (cm^{-1}): 3054 (vw), 2924 (vw), 2854 (vw), 1434 (s), 1260 (s), 1223 (w), 1145 (m), 1099 (m), 1029 (s), 999 (m), 816 (m), 741 (m), 688 (vs), 635 (vs), 530 (s), 516 (s), 481 (s). UV/Vis λ_{max} (dichloromethane): 226 nm (major, ε = 47 609 M^{-1} cm^{-1}), 259 nm (shoulder, ε = 32 171 M^{-1} cm^{-1}), 332 nm (minor, ε = 21 752 M^{-1} cm^{-1}). ESI-TOF-MS (3 kV, dichloromethane): m/z calcd for [(κ^1-dppe)PdCl(κ^1dpph)]$^+$, 993.2; expt., 993.3 (100%). m/z calcd for [(κ^2-dppe)PdCl]$^+$, 541.0; expt., 541.0 (43%).

General procedure for the synthesis of [(κ^2-dppe)PtCl(κ^1-dppx)](OTf) (Pt-x)

A solution of 200 mg (0.125 mmol, 1.00 eq.) of **PtPt-0** in 6 mL dichloromethane was added to a solution containing two equivalents of the respective diphosphine in 6 mL of dichloromethane. It was then left to stir for 1 h at room temperature. The solvents were removed *in vacuo*, the solids were then washed with diethyl ether and dried *in vacuo*. The products are obtained as off white solids.

Characterisation of [(κ^2-dppe)PtCl(κ^1-dppb)](OTf) (Pt-1)

220 mg (72%) of off-white solid, air stable. Melting point: 117 °C. ^{1}H NMR (400.130 MHz, DMSO-d_6, 293 K): δ 7.90–7.06 (40 H, unresolved m, P*Ph*), 2.73 (2 H, unresolved m, PCH_2^ACH_2^BP, κ^2-dppe), 2.46 (signal obscured by solvent) (2 H, obscured m, PCH_2^ACH_2^BP, κ^2-dppe), 2.30 (3 H, unresolved m, CH_2, dppb), 1.92 (1 H, t, $^xJ_{\text{H–X}}$ = 7.81 Hz, CH_2, dppb), 1.62–1.19 (4 H, unresolved m, 2 × CH_2, dppb). ^{13}C{^{1}H} (100.613 MHz, DMSO-d_6, 293 K): δ 138.3 (d, $^xJ_{\text{C–P}}$ = 13.6 Hz, P*Ph*), 132.9 (unresolved m, P*Ph*), 131.2 (d, $^xJ_{\text{C–P}}$ = 12.9 Hz, P*Ph*), 128.8 (unre-

solved m, P*Ph*), 124.7 (d, $^xJ_{C-P}$ = 17.3 Hz, P*Ph*), 124.1 (d, $^xJ_{C-P}$ = 17.3 Hz, P*Ph*), 120.7 (d, $^xJ_{C-P}$ = 322.3 Hz, P*Ph*), 32.7 (br s, PC^AH$_2$$C^BH_2$P, κ^2-dppe), 26.8 (s, dppb), 26.2 (d, $^xJ_{C-P}$ = 12.3 Hz, dppb), 24.2 (br s, dppb + PC^AH2C^BH2P, κ^2-dppe). ^{31}P{^{1}H} (161.976 MHz, DMSO-d_6, 293 K): δ 53.82 (dd, $^1J_{PA-Pt}$ = 2369.0 Hz, $^2J_{PA-PC}$ = 380.8 Hz, $^2J_{PA-PB}$ = 5.53 Hz, P^A, conformer A), 53.79 (dd, $^1J_{PA-Pt}$ = 2369.0 Hz, $^2J_{PA-PC}$ = 380.2 Hz, $^2J_{PA-PB}$ = 5.57 Hz, P^A, conformer B), 44.84 (dd, $^1J_{PB-Pt}$ = 3512.2 Hz, $^2J_{PB-PC}$ = 16.14 Hz, $^2J_{PB-PA}$ = 5.61 Hz, P^B, conformer X), 44.77 (dd, $^1J_{PB-Pt}$ = 3512.2 Hz, $^2J_{PB-PC}$ = 16.14 Hz, $^2J_{PB-PA}$ = 5.61 Hz, P^B, conformer X), 17.3 (dd, $^1J_{PC-Pt}$ = 2374.6 Hz, $^2J_{PC-PA}$ = 380.40 Hz, $^2J_{PC-PB}$ = 16.24 Hz, P^C, conformer A), 17.16 (dd, $^1J_{PC-Pt}$ = 2374.6 Hz, $^2J_{PC-PA}$ = 380.02 Hz, $^2J_{PC-PB}$ = 16.1 Hz, P^C, conformer B), −16.72 (br s, $Δν_{1/2}$ = 51.28 Hz, P^D, conformer A), −17.48 (s, P^D, conformer B). ^{19}F (376.498 MHz, DMSO-d_6, 293 K): δ −77.6 (OTf). FTIR (cm^{-1}): 3054 (w), 1482 (w), 1435 (m), 1260 (s), 1146 (m), 1102 (s), 1030 (s), 744 (s), 690 (s), 636 (s), 532 (s), 515 (s), 486 (s), 442 (m). ESI-TOF-MS (3 kV, dichloromethane): *m/z* calcd [(κ^2-dppe)PtCl(κ^1-dppb)O]$^+$, 1071.2; expt., 1071.1 (36.2%); calcd [(κ^2-dppe)PtCl(κ^1-dppb)]$^+$, 1055.2; expt., 1055.1 (100%); calcd [PtCl(κ^1-dppb)]OTf-H$^+$, 842.0; expt., 842.1 (3.67%).

Characterisation of [(κ^2-dppe)PtCl(κ^1-dpppent)](OTf) (Pt-2)

248 mg (81%) of white powder, air stable. ^{1}H NMR (400.130 MHz, DMSO-d_6, 293 K): δ 7.87–7.13 (40 H, unresolved m, P*Ph*), 2.73 (2 H, unresolved m, PCH_2^{A}CH_2^{B}P, κ^2-dppe), 2.37 (4 H, unresolved m, 1 × CH_2, dpppent + PCH_2^{A}CH_2^{B}P, κ^2-dppe), 1.98 (2 H, ps q, 1 × CH_2, dpppent), 1.30 (6 H, unresolved m, 3 × CH_2, dpppent). ^{13}C{^{1}H} NMR (100.613 MHz, DMSO-d_6, 293 K): δ 138.8–128.0 (unresolved m, P*Ph*), 126.9 (d, $^xJ_{C-P}$ = 57.3 Hz, P*Ph*), 124.4 (d, $^xJ_{C-P}$ = 62.4 Hz, P*Ph*), 122.3 (s, P*Ph*), 119.1 (s, P*Ph*), 32.8 (br s, PC^AH$_2$$C^BH_2$P, κ^2-dppe), 31.5 (br s, dpppent), 26.4 (unresolved m, dpppent), 24.6 (unresolved m, dpppent + PC^AH$_2$$C^BH_2$P, κ^2-dppe). ^{31}P{^{1}H} NMR (161.976 MHz, DMSO-d_6, 293 K): δ 53.93 (dd, $^1J_{PA-Pt}$ = 2366.1 Hz, $^2J_{PA-PC}$ = 379.0 Hz, $^2J_{PA-PB}$ = 5.9 Hz, P^A, conformer A), 53.88 (dd, $^1J_{PA-Pt}$ = 2366.1 Hz, $^2J_{PA-PC}$ = 380.1 Hz, $^2J_{PA-PB}$ = 5.6 Hz, P^A, conformer B), 45.0 (dd, $^1J_{PB-Pt}$ = 3514.0 Hz, $^2J_{PB-PC}$ = 15.4 Hz, $^2J_{PB-PA}$ = 5.7 Hz, P^B, conformer A), 44.9 (dd, $^1J_{PB-Pt}$ = 3514.0 Hz, $^2J_{PB-PC}$ = 16.1 Hz, $^2J_{PB-PA}$ = 5.7 Hz, P^B, conformer B), 17.2 (dd, $^1J_{PC-Pt}$ = 2368.5 Hz, $^2J_{PC-PA}$ = 379.8 Hz, $^2J_{PC-PB}$ = 16.1 Hz, P^C, conformer B), 16.9 (dd, $^1J_{PC-Pt}$ = 2374.9 Hz, $^2J_{PC-PA}$ = 379.0 Hz, $^2J_{PC-PB}$ = 16.0 Hz, P^C, conformer A), −16.87 (s, P^D, conformer B), −16.94 (obscured s, P^D, conformer A). ^{19}F NMR (376.498 MHz, DMSO-d_6, 293 K): δ −77.6 (OTf). FTIR (cm^{-1}): 3056 (w), 2931 (w), 2852 (w), 1435 (m), 1261 (s), 1223 (m), 1147 (m), 1102 (m), 1030 (s), 999 (m), 742 (m), 690 (s), 636 (s), 533 (s), 488 (s). ESI-TOF-MS (3 kV, dichloromethane): *m/z* calcd [(κ^2-dppe)PtCl(κ^1-dppp)O]$^+$, 1085.2; expt., 1085.2 (10.0%); calcd [(κ^2-dppe)PtCl(κ^1-dppp)]$^+$, 1069.2; expt., 1069.2 (100%); calcd [PtCl(κ^1-dppp)]OTf-H$^+$, 842.0; expt., 842.1 (3.67%).

Characterisation of [(κ^2-dppe)PtCl(κ^1-dpph)](OTf) (Pt-3)

^{1}H NMR (400.130 MHz, DMSO-d_6, 293 K): δ 7.88–7.14 (40 H, unresolved m, P*Ph*), 2.73 (2 H, unresolved m, 1 × CH$_2$, PCH_2^{A}CH$_2$^{B}P, κ^2-dppe), 2.46 (signal obscured by solvent) (2 H,

obscured m, 1 × CH$_2$, PCH$_2$^{A}CH_2^{B}P, κ^2-dppe), 2.34 (3 H, unresolved m, CH_2, dpph), 2.01 (2 H, unresolved m, 1 × CH$_2$, dpph), 1.26 (7 H, unresolved m, CH$_2$, dpph). ^{13}C{^{1}H} NMR (100.613 MHz, acetone-d_6, 293 K): δ 135.2–128.5 (unresolved m, P*Ph*), 31.2 (unresolved m, CH$_2$, dpph), 26.1 (br s, PCH$_2$CH$_2$P, κ^2-dppe). ^{31}P{^{1}H} NMR (161.976 MHz, acetone-d_6, 293 K): δ 53.6 (dd, $^1J_{PA-Pt}$ = 2353.4 Hz, $^2J_{PA-PC}$ = 383.5, $^2J_{PA-PB}$ = 6.53 Hz, P^A, conformer A), 53.5 (dd, $^1J_{PA-Pt}$ = 2353.4 Hz, $^2J_{PA-PC}$ = 382.5 Hz, $^2J_{PA-PB}$ = 6.15 Hz, P^A, conformer B), 45.0 (dd, $^1J_{PB-Pt}$ = 3506 Hz, $^2J_{PB-PC}$ = 16.11 Hz, $^2J_{PB-PA}$ = 6.25, P^B), 17.2 (dd, $^2J_{PC-Pt}$ = 2349.8 Hz, $^2J_{PC-PA}$ = 382.0 Hz, $^2J_{PC-PB}$ = 16.55, P^C, conformer A + B), −15.8 (s, P^D, conformer A), −16.4 (s, P^D, conformer B). ^{19}F NMR (376.498 MHz, acetone-d_6, 293 K): δ −78.6 (OTf). FTIR (cm^{-1}): 3055 (w), 2924 (w), 2857 (w), 1742 (w), 1435 (m), 1260 (s), 1223 (m), 1147 (s), 1101 (s), 1030 (s), 999 (m), 822 (m), 743 (s), 690 (s), 636 (s), 532 (s), 516 (s), 485 (s). UV/Vis $λ_{max}$ (dichloromethane): 226 nm (major, ε = 154 941 M^{-1} cm^{-1}), 274 nm (shoulder, ε = 61 601 M^{-1} cm^{-1}). ESI-TOF-MS (3 kV, dichloromethane): *m/z* calcd [(κ^2-dppe)PtCl(κ^1-dpph)O]$^+$, 1099.3; expt., 1099.2 (36.2%); calcd [(κ^2-dppe)PtCl(κ^1-dpph)]$^+$, 1083.3; expt., 1083.2 (100%).

General procedure for the synthesis of [((κ^2-dppe)PdCl)$_2$(μ-dppx)](2OTf) (PdPd-x)

200 mg (0.140 mmol, 1.00 eq.) of **PdPd-0** and 0.140 mmol (1.00 eq.) of diphosphine were added as solids in a Schlenk flask, which was subsequently purged through vacuum/N$_2$ cycles. 30 mL of dried, degassed DCM were then added and the solution was stirred at room temperature for 1 h. The solvents were removed *in vacuo*, after which the solids were washed with 3 × 10 mL dry Et$_2$O, and subsequently dried *in vacuo*.

Characterisation of [((κ^2-dppe)PdCl)$_2$(μ-dppb)](2OTf) (PdPd-1)

169.3 mg (67%) of light yellow solid, air stable. Melting point: 211 °C + dec. ^{1}H NMR (400.130 MHz, DMSO-d_6, 298 K): δ 7.83–7.14 (60 H, unresolved m, P*Ph*), 2.84 (4 H, ps dd, $^2J_{H-P}$ = 34.9 Hz, $^3J_{H-P}$ = 6.2 Hz, PCH_2^{A}CH$_2$^{B}P, κ^2-dppe), 2.47 (obscured by solvent, 4 H, ps d, PCH$_2$^{A}CH_2^{B}P, κ^2-dppe), 2.17 (4 H, br s, $Δν_{1/2}$ = 24.2 Hz, 2 × CH$_2$, dppb), 1.28 (4 H, br s, $Δν_{1/2}$ = 20.4 Hz, 2 × CH$_2$, dppb). ^{13}C NMR (100.613 MHz, DMSO-d_6, 298 K): δ 133.5 (d, $^xJ_{C-P}$ = 10.7 Hz, P*Ph*), 133.3 (d, $^xJ_{C-P}$ = 11.7 Hz, P*Ph*), 132.9 (d, $^xJ_{C-P}$ = 10.6 Hz, P*Ph*), 132.3 (s, P*Ph*), 131.1 (s, P*Ph*), 129.4 (d, $^xJ_{C-P}$ = 11.1 Hz, P*Ph*), 129.2 (d, $^xJ_{C-P}$ = 11.0 Hz, P*Ph*), 128.7 (d, $^xJ_{C-P}$ = 10.2 Hz, P*Ph*), 128.0 (d, $^xJ_{C-P}$ = 43.5 Hz, P*Ph*), 127.8 (d, $^xJ_{C-P}$ = 49.6 Hz, P*Ph*), 125.2 (d, $^xJ_{C-P}$ = 52.6 Hz, P*Ph*), 120.7 (d, $^xJ_{C-P}$ = 322.3 Hz, P*Ph*), 32.7 (ps dd, $^1J_{C-P}$ = 37.1 Hz, $^2J_{C-P}$ = 18.1 Hz, PC^AH$_2$$C^BH_2$P, κ^2-dppe), 26.2 (d, $^2J_{C-P}$ = 14.3 Hz, μ-dppb-PC^AH$_2$$C^BH_2$), 24.6 (d, $^1J_{C-P}$ = 26.4 Hz, μ-dppb-PC^AH$_2$$C^BH_2$), 24.3–23.8 (m, P$C^AH_2$$C^BH_2$P, κ^2-dppe). ^{31}P NMR (161.976 MHz, DMSO-d_6, 298 K): δ 66.0 (br s, $Δν_{1/2}$ = 24.2 Hz, P^B), 64.81 (dd, $^2J_{PA-PC}$ = 431.2 Hz, $^2J_{PA-PB}$ = 6.8 Hz, P^A), 17.9 (dd, $^2J_{PC-PA}$ = 411.3, $^2J_{PC-PB}$ = 17.8, P^C). ^{19}F NMR (376.498 MHz, DMSO-d_6, 298 K): δ −77.7 (OTf). FT-IR (cm^{-1}): 3057 (w), 1484 (w), 1436 (m), 1262 (s), 1223 (m), 1147 (m), 1101 (m), 1030 (m), 999 (m), 879 (w), 813 (w), 742 (m), 690 (s), 635 (s). UV-Vis $λ_{max}$

(dichloromethane): 226 nm (major, ε = 103 695 M^{-1} cm^{-1}), 267 nm (shoulder, ε = 42 876 M^{-1} cm^{-1}), 332 nm (minor, ε = 38 438 M^{-1} cm^{-1}). ESI-TOF-MS: m/z calcd for $[M-OTf]^+$, 1656.1; expt., 1656.3.

Characterisation of [((κ²-dppe)PdCl)₂(μ-dpppent)](2OTf) (PdPd-2)

170.2 mg (67%) of light yellow solid, air stable. ^1H NMR (400.130 MHz, DMSO-d_6, 298 K): δ 7.84–7.15 (60 H, unresolved m, P*Ph*), 2.83 (4 H, ps dd, $^2J_{H-P}$ = 34.9 Hz, $^3J_{H-P}$ = 6.4 Hz, PC*H₂*^{A}C*H₂*^{B}P, κ²-dppe), 2.48 (obscured by solvent, 4 H, ps d, PC*H₂*^{A}C*H₂*^{B}P, κ²-dppe), 2.27 (4 H, br s, $\Delta\nu_{1/2}$ = 25.1 Hz, 2 × C*H₂*, dpppent-C*H₂*^{A}), 1.21 and 1.16 (6 H, br s, overlapped signals, 2 × C*H₂*, dpppent-C*H₂*^{B} and dpppent-C*H₂*^{C}). ^{13}C NMR (100.613 MHz, DMSO-d_6, 298 K): δ 133.5 (d, $^xJ_{C-P}$ = 10.5 Hz, P*Ph*), 133.3 (d, $^xJ_{C-P}$ = 11.8 Hz, P*Ph*), 132.9 (d, $^xJ_{C-P}$ = 9.1 Hz, P*Ph*), 132.3 (s, P*Ph*), 131.1 (s, P*Ph*), 129.4 (d, $^xJ_{C-P}$ = 11.1 Hz, P*Ph*), 129.1 (d, $^xJ_{C-P}$ = 11.1 Hz, P*Ph*), 128.6 (d, $^xJ_{C-P}$ = 10.0 Hz, P*Ph*), 128.0 (s, P*Ph*), 128.0 (d, $^xJ_{C-P}$ = 95.1 Hz, P*Ph*), 125.2 (d, $^xJ_{C-P}$ = 52.7 Hz, P*Ph*), 120.7 (d, $^xJ_{C-P}$ = 322.3 Hz, P*Ph*), 32.7 (ps dd, $^1J_{C-P}$ = 34.5 Hz, $^2J_{C-P}$ = 14.5 Hz, PC^{A}H₂C^{B}H₂P, κ²-dppe), 31.7–31.3 (m, dpppent-P*C*H₂CH₂CH₂), 25.0 (d, $^2J_{C-P}$ = 25.1 Hz, dpppent-P*C*H₂CH₂CH₂), 24.2 (s, dpppent-PCH₂CH₂*C*H₂), 24.4–23.9 (m, PC^{A}H₂*C^{B}H₂P, κ²-dppe). ^{31}P NMR (161.976 MHz, DMSO-d_6, 298 K): δ 66.1 (dd, $^2J_{Px-Px}$ = 38.9 Hz, $^2J_{Px-Px}$ = 7.4 Hz, P^B), 64.9 (dd, $^2J_{PA-Pc}$ = 467.5 Hz, $^2J_{PA-PB}$ 7.3 Hz, P^A), 17.8 (dd, $^2J_{PC-PA}$ = 410.1 Hz, $^2J_{PC-PB}$ = 19.0, P^C). ^{19}F NMR (376.498 MHz, DMSO-d_6, 298 K): δ −77.6 (OTf). FTIR (cm^{-1}): 3056 (w), 1586 (w), 1574 (w), 1436 (m), 1410 (w), 1312 (w), 1262 (s), 1223 (m), 1147 (m), 1101 (m), 1030 (s), 999 (m), 879 (w), 844 (w), 813 (w), 741 (m), 716 (m), 704 (m), 688 (s), 657 (m), 635 (s), 616 (m). UV-Vis λ_{max} (dichloromethane): 225 nm (major, ε = 101 105 M^{-1} cm^{-1}), 266 nm (shoulder, ε = 42 676 M^{-1} cm^{-1}), 331 nm (minor, ε = 34 038 M^{-1} cm^{-1}).

Characterisation of [((κ²-dppe)PdCl)₂(μ-dpph)](2OTf) (PdPd-3)

182 mg (71%) of light yellow solid, air stable. ^1H NMR (400.130 MHz, DMSO-d_6, 298 K): δ 7.85–7.17 (60 H, unresolved m, P*Ph*), 2.85 (4 H, ps dd, $^2J_{H-P}$ = 34.9 Hz, $^3J_{H-P}$ = 6.4 Hz, 2 × CH₂, PC*H₂*^{A}C*H₂*^{B}P, κ²-dppe), 2.50 (obscured by solvent, 4 H, ps d, 2 × CH₂, PC*H₂*^{A}C*H₂*^{B}P, κ²-dppe), 2.30 (4 H, br s, $\Delta\nu_{1/2}$ = 25.6 Hz, 2 × dpph-C*H₂*), 1.23 (4 H, br s, $\Delta\nu_{1/2}$ = 26.2 Hz, 2 × dpph-C*H₂*), 1.06 (obscured by Et₂O signal, 4 H, br s, $\Delta\nu_{1/2}$ = 14.8 Hz, 2 × dpph-C*H₂*). ^{13}C NMR (100.613 MHz, DMSO-d_6, 298 K): δ 133.5 (d, $^xJ_{C-P}$ = 10.6 Hz, P*Ph*), 133.3 (d, $^xJ_{C-P}$ = 11.7 Hz, P*Ph*), 132.8 (d, $^xJ_{C-P}$ = 10.3 Hz, P*Ph*), 132.6 (d, $^xJ_{C-P}$ = 58.7 Hz, P*Ph*), 131.0 (s, P*Ph*), 129.5 (d, $^xJ_{C-P}$ = 11.1 Hz, P*Ph*), 129.2 (d, $^xJ_{C-P}$ = 11.0 Hz, P*Ph*), 128.6 (d, $^xJ_{C-P}$ = 10.3 Hz, P*Ph*), 127.8 (d, $^xJ_{C-P}$ = 50.5 Hz, P*Ph*), 125.2 (d, $^xJ_{C-P}$ = 51.3 Hz, P*Ph*), 120.7 (d, $^xJ_{C-P}$ = 321.7 Hz, P*Ph*), 33.1–32.3 (m, PC^{A}H₂C^{B}H₂P, κ²-dppe), 29.8 (d, $^2J_{C-P}$ = 14.2 Hz, dpph-P*C*H₂CH₂CH₂), 25.2–24.6 (m, overlapping signals, dpph-PCH₂*C*H₂CH₂ and dpph-PCH₂CH₂*C*H₂), 24.4–23.8 (m, PC^{A}H₂*C^{B}H₂P, κ²-dppe). ^{31}P NMR (161.976 MHz, DMSO-d_6, 298 K): δ 66.1 (dd, $^2J_{Px-Px}$ = 32.7 Hz, $^2J_{Px-Px}$ = 7.3 Hz, P^B), 64.9 (dd, $^2J_{PA-Pc}$ = 462.1 Hz, $^2J_{PA-PB}$ = 7.3 Hz, P^A), 18.0 (dd, $^2J_{PC-PA}$ = 411.0 Hz, $^2J_{PC-PB}$ = 19.1, P^C). ^{19}F NMR (376.498 MHz,

DMSO-d_6, 298 K): δ −77.6 (OTf). FTIR (cm^{-1}): 3055 (w), 2927 (w), 1586 (w), 1574 (w), 1483 (w), 1436 (m), 1408 (w), 1311 (w), 1259 (s), 1223 (m), 1188 (w), 1145 (m), 1099 (m), 1029 (s), 999 (m), 881 (w), 819 (w), 743 (m), 714 (m), 704 (m), 688 (s), 657 (m), 635 (s), 616 (m). UV-Vis λ_{max} (dichloromethane): 226 nm (major, ε = 104 209 M^{-1} cm^{-1}), 266 nm (shoulder, ε = 44 857 M^{-1} cm^{-1}), 331 nm (minor, ε = 35 485 M^{-1} cm^{-1}). TOF-MS: m/z calcd for $[M-OTf]^+$, 1684.2; expt., 1684.3.

General procedure for the synthesis of [(κ²-dppe)ClPd(μ-dppx)RuCl₂(η⁶-p-cym)](OTf) (PdRu-x)

26.8 mg (0.044 mmol, 1.00 eq.) of [(η⁶-p-cym)RuCl₂]₂ dimer was dissolved in dichloromethane (10 mL) in a Schlenk flask. Similarly, **Pd-x** (0.087 mmol, 2.00 eq.) was dissolved in dichloromethane (10 mL) and added rapidly to the Ru dimer solution while stirring. The resulting solution was left to stir at room temperature for two hours. The solvent was removed *in vacuo*, after which the resulting solid was washed with diethyl ether (10 mL), and the washings discarded. The product was subsequently dried *in vacuo* overnight.

Characterisation of [(κ²-dppe)ClPd(μ-dppx)RuCl₂(η⁶-p-cym)] (OTf) (PdRu-1)

117 mg (69%) of brick-red solid, air stable. Melting point: 165–170 °C, 180 °C + (dec.). ^1H NMR (400.130 MHz, DMSO-d_6, 298 K): δ 7.92–7.10 (40 H, unresolved m, P*Ph*), 5.42 (2 H, ps d, 2 × C*H*, −C^{3,5}-*H*, p-cymene, conformer B), 5.36 (d, $^3J_{H-H}$ = 5.9 Hz, 2 × C*H*, −C^{3,5}-*H*, p-cymene, conformer A), 5.21 (2 H, ps d, 2 × C*H*, −C^{2,6}-*H*, p-cymene conformer B), 5.17 (d, $^3J_{H-H}$ = 5.6 Hz, 2 × C*H*, −C^{2,6}-*H*, conformer A), 2.81 (2 H, ps d, $^2J_{H-P}$ = 36.7 Hz, PC*H₂*^{A}C*H₂*^{B}P, κ²-dppe), 2.45 (obscured by solvent) (2 H, obscured br d, PC*H₂*^{A}C*H₂*^{B}P, κ²-dppe), 2.35–1.85 (5 H, unresolved m, 2 × CH₂ + 1 × −C*H*(CH₃)₂, dppb + p-cymene), 1.76 (3 H, s, 1 × −C(C*H₃*), p-cymene, conformer B), 1.70 (s, 1 × −C(C*H₃*), p-cymene, conformer A), 1.32–1.11 (2 H, ps d, 1 × C*H₂*, dppb), 0.96–0.84 (2 H, br s, $\Delta\nu_{1/2}$ = 23.6 Hz, 1 × C*H₂*, dppb), 0.74 (6 H, ps d, $^3J_{H-H}$ = 7.4 Hz, 1 × −CH(C*H₃*)₂, p-cymene, conformer B), 0.72 (ps d, $^3J_{H-H}$ = 7.2 Hz, 1 × −CH(C*H₃*)₂, p-cymene, conformer A). $^{13}C\{^1H\}$ NMR (100.613 MHz, DMSO-d_6, 298 K): δ 133.8–127.4 (unresolved m, P*Ph*), 106.3 (br ps d, $\Delta\nu_{1/2}$ = 10.1 Hz, −*C^1*, p-cymene, conformer A + B), 93.5 (br ps d, $\Delta\nu_{1/2}$ = 10.5 Hz, −*C^4*, p-cymene, conformer A + B), 90.2 (br s, $\Delta\nu_{1/2}$ = 9.8 Hz, 2 × C*H*, −C^{3,5}-*H*, p-cymene, conformer A + B), 85.5 (br s, $\Delta\nu_{1/2}$ = 10.9 Hz, 2 × C*H*, −C^{2,6}-*H*, p-cymene, conformer A + B), 32.6 (PC^{A}H₂C^{B}H₂P, κ²-dppe), 29.5 (br m, $\Delta\nu_{1/2}$ = 9.7 Hz, 1 × −*C*H(CH₃)₂, p-cymene, conformer A + B), 26.6 (1 × *C*H₂, dppb), 26.2 (1 × *C*H₂, dppb), 24.4 (1 × *C*H₂, dppb), 24.1 (1 × *C*H₂, dppb), 23.2 (PC^{A}H₂C^{B}H₂P, κ²-dppe), 21.0 (br s, $\Delta\nu_{1/2}$ = 9.9 Hz, 1 × −*C*H(CH₃)₂, p-cymene, conformers A + B), 17.0 (br s, $\Delta\nu_{1/2}$ = 10.0 Hz, 1 × −C(*C*H₃), conformer A + B). $^{31}P\{^1H\}$ NMR (161.976 MHz, DMSO-d_6, 298 K): δ 66.2–65.9 (ps dd, P^B, conformer A + B), 64.7 (dd, $^2J_{PA-Pc}$ = 390.9 Hz, $^2J_{PA-PB}$ = 7.2 Hz, P^A, conformer B), 64.5 (ps dd, $^2J_{PA-Pc}$ = 329.9 Hz, $^2J_{PA-PB}$ = 7.3 Hz, P^A, conformer A), 23.7 (br s, $\Delta\nu_{1/2}$ = 3.9 Hz, P^D, conformer B), 23.3 (br s, $\Delta\nu_{1/2}$ = 2.7 Hz, P^D, conformer A), 17.8 (ps dd, $^2J_{PC-PA}$ = 412.2 Hz, $^2J_{PC-PB}$ = 20.3 Hz, P^C, conformer B), 17.7 (dd, $^2J_{PC-PA}$

= 415.4 Hz, $^2J_{PC–PB}$ = 20.9 Hz, P^C, conformer A). ^{19}F NMR (376.498 MHz, DMSO-d_6, 298 K): δ = −77.6 (OTf). FTIR (cm^{-1}): 3055 (vw), 2959 (vw), 2868 (vw), 1434 (m), 1260 (s), 1147 (m), 1099 (m), 1030 (s), 997 (w), 743 (m), 690 (vs), 637 (vs), 529 (vs), 516 (s), 483 (m). UV/Vis λ_{max} (dichloromethane): 226 nm (major), 266 nm (shoulder), 332 nm (minor), 488 (weak, forbidden d–d). ESI-TOF-MS (3 kV, dichloromethane): m/z calcd for [(κ^2-dppe)PdCl(μ-dppb)RuCl$_2$(η^6-p-cymene)]$^+$, 1273.1; expt., 1273.3 (55%). m/z calcd for [(κ^2-dppe)PdCl(κ^1-dppb)O]$^+$, 981.2; expt., 981.3 (31%). m/z calcd for [(κ^2-dppe)PdCl(κ^1-dppb)]$^+$, 965.2 expt., 965.3 (100%). m/z calcd for [(η^6-p-cymene)RuCl(κ^1-dppb)O]$^+$, 713.2; expt. 713.2 (4%). m/z calcd for [(η^6-p-cymene)RuCl(κ^1-dppb)]$^+$, 697.2; expt. 697.2 (12%). m/z calcd for [(κ^2-dppe)PdCl]$^+$, 541.0; expt., 541.0 (28%).

Characterisation of [(κ^2-dppe)ClPd(μ-dppx)RuCl$_2$(η^6-p-cym)] (OTf) (PdRu-2)

235.5 mg (85%) of brick-red solid, air stable. ^{1}H NMR (400.130 MHz, DMSO-d_6, 298 K): δ 7.90–7.10 (40 H, unresolved m, PPh), 5.42 (2 H, d, $^3J_{H–H}$ = 5.8 Hz, 2 × CH, –C^{3,5}–H, p-cymene, conformer B), 5.37 (d, $^3J_{H–H}$ = 6.1 Hz, 2 × CH, –C^{3,5}–H, p-cymene, conformer A), 5.23 (2 H, d, $^3J_{H–H}$ = 6.2 Hz, 2 × CH, –C^{2,6}–H, conformer B), 5.19 (d, $^3J_{H–H}$ = 6.2 Hz, 2 × CH, –C^{2,6}–H, conformer A), 2.82 (2 H, m, PCH_2^ACH_2^BP, κ^2-dppe), 2.47 (obscured by solvent) (2 H, obscured br m, PCH_2^ACH_2^BP, κ^2-dppe), 2.41–2.00 (5 H, unresolved m, 2 × CH_2 + 1 × –CH(CH$_3$)$_2$, dppp + p-cymene), 1.77 (3 H, s, 1 × –C(CH_3), p-cymene, conformer B), 1.71 (s, 1 × –C(CH_3), p-cymene, conformer A), 1.28–0.98 (4 H, unresolved m, 2 × CH_2, dppp), 0.94–0.81 (2 H, br m, $\Delta\nu_{1/2}$ = 22.1 Hz, 1 × CH_2, dppp), 0.74 (6 H, ps d, $^3J_{H–H}$ = 7.4 Hz, 1 × –CH(CH_3)$_2$, p-cymene, conformer B), 0.72 (ps d, $^3J_{H–H}$ = 7.2 Hz, 1 × –CH(CH_3)$_2$, conformer A). ^{13}C{^{1}H} NMR (100.613 MHz, DMSO-d_6, 298 K): δ 133.7–127.3 (unresolved m, PPh), 106.3 (s, 1 × –C^1, p-cymene, conformer B), 106.2 (s, 1 × –C^1, p-cymene, conformer A), 93.3 (s, 1 × –C^4, p-cymene, conformer B), 93.2 (s, 1 × –C^4, p-cymene, conformer A), 90.34 (ps d, $^2J_{C–P}$ = 4.3 Hz, 2 × CH, –$C^{3,5}$–H, p-cymene, conformer B), 90.28 (ps d, $^2J_{C–P}$ = 4.3 Hz, 2 × CH, –$C^{3,5}$–H, conformer A), 85.4 (d, $^2J_{C–P}$ = 6.0 Hz, 2 × CH, –$C^{3,5}$–H, p-cymene, conformer B), 85.2 (d, $^2J_{C–P}$ = 6.0 Hz, 2 × CH, –$C^{3,5}$–H, conformer B), 32.6 (PCH_2^ACH_2^BP, κ^2-dppe), 31.4 (1 × CH$_2$, dppp), 29.49 (s, 1 × –CH(CH$_3$)$_2$, p-cymene, conformer B), 29.48 (s, 1 × –CH(CH$_3$)$_2$, p-cymene, conformer A), 24.8 (s, 1 × CH$_2$, dppp), 23.4 (PCH_2^ACH_2^BP, κ^2-dppe), 23.1 (1 × CH$_2$, dppp), 22.3 (1 × CH$_2$, dppp), 22.1 (1 × CH$_2$, dppp), 20.9 (br s, $\Delta\nu_{1/2}$ = 1.4 Hz, 1 × –CH(CH_3)$_2$, p-cymene, conformers A + B), 17.0 (s, 1 × –C(CH_3), p-cymene, conformer B), 16.9 (s, 1 × –C(CH_3), p-cymene, conformer A). ^{31}P{^{1}H} NMR (161.976 MHz, DMSO-d_6, 298 K): δ 66.3 (ps dd (partially hidden by conformer A), $^2J_{PB–PC}$ = 19.1 Hz, $^2J_{PB–PA}$ = 7.5 Hz, P^B, conformer B), 66.2 (dd, $^2J_{PB–PC}$ = 19.1 Hz, $^2J_{PB–PA}$ = 7.5 Hz, P^B, conformer A), 64.7 (dd, $^2J_{PA–PC}$ = 410.7 Hz, $^2J_{PA–PB}$ = 7.2 Hz, P^A, conformer B), 64.6 (dd, $^2J_{PA–PC}$ = 410.8 Hz, $^2J_{PA–PB}$ = 7.3 Hz, P^A, conformer B), 23.7 (s, P^D, conformer B), 23.3 (s, P^D, conformer A), 17.8 (dd, $^2J_{PC–PA}$ = 410.8 Hz, $^2J_{PC–PB}$ = 19.1 Hz, P^C, conformer B), 17.7 (dd, $^2J_{PC–PA}$ = 411.3 Hz, $^2J_{PC–PB}$ = 19.7 Hz, P^C,

conformer A). ^{19}F NMR (376.498 MHz, DMSO-d_6, 298 K): δ −77.6 (1 × CF_3SO$_3$, OTf$^-$). FTIR (cm^{-1}): 3054 (vw), 2924 (vw), 1436 (m), 1262 (s), 1148 (m), 1099 (m), 1030 (s), 997 (w), 743 (m), 691 (vs), 637 (vs), 529 (vs), 516 (s), 483 (m). UV/Vis λ_{max} (dichloromethane): 226 nm (major, ε = 105 543 M^{-1} cm^{-1}), 268 nm (shoulder, ε = 38 971 M^{-1} cm^{-1}), 331 nm (minor, ε = 25 124 M^{-1} cm^{-1}), 487 (weak, forbidden d–d). ESI-TOF-MS (3 kV, dichloromethane): m/z calcd for [(κ^2-dppe)PdCl(μ-dppp)RuCl$_2$(η^6-p-cymene)]$^+$, 1287.1; expt., 1287.1 (77%). m/z calcd for [(κ^2-dppe)PdCl(κ^1-dppp)O]$^+$, 995.2; expt., 995.2 (100%). m/z calcd for [(κ^2-dppe)PdCl(κ^1-dppp)]$^+$, 979.2; expt., 979.2 (8%). m/z calcd for [(η^6-p-cymene)RuCl(κ^1-dppp)]$^+$, 711.2; expt. 711.2 (76%). m/z calcd for [(κ^2-dppe)PdCl]$^+$, 541.0; expt., 541.1 (39%).

Characterisation of [(κ^2-dppe)ClPd(μ-dppx)RuCl$_2$(η^6-p-cym)] (OTf) (PdRu-3)

83 mg (65%) of brick-red solid, air stable. ^{1}H NMR (400.130 MHz, DMSO-d_6, 298 K): δ 7.85–7.15 (40 H, unresolved m, PPh), 5.42 (2 H, d, $^3J_{H–H}$ = 6.2 Hz, 2 × CH, –C^{3,5}–H, conformer B), 5.38 (d, $^3J_{H–H}$ = 6.5 Hz, 2 × CH, –C^{3,5}–H, conformer A), 5.21 (2 H, d, $^3J_{H–H}$ = 6.0 Hz, 2 × CH, C^{2,6}–H, p-cymene, conformer B), 5.19 (d, $^3J_{H–H}$ = 6.1 Hz, 2 × CH, –C^{2,6}–H, conformer A), 2.84 (2 H, m, PCH_2^ACH_2^BP, κ^2-dppe), 2.44 (obscured by solvent) (2 H, obscured br d, PCH_2^ACH_2^BP, κ^2-dppe), 2.39–1.88 (5 H, unresolved m, 2 × CH_2 + 1 × –CH(CH$_3$)$_2$, dpph + p-cymene), 1.76 (3 H, s, 1 × –C(CH_3), p-cymene, conformer B), 1.73 (s, 1 × –C(CH_3), p-cymene, conformer A), 1.29–1.19 (2 H, br s, $\Delta\nu_{1/2}$ = 19.9 Hz, 1 × CH_2, dpph), 1.18–1.02 (2 H, br m, $\Delta\nu_{1/2}$ = 14.2 Hz, 1 × CH_2, dpph), 0.89 (4 H, ps d, 2 × CH_2, dpph), 0.72 (6 H, d, $^3J_{H–H}$ = 7.0 Hz, 1 × –CH(CH_3)$_2$, p-cymene, conformer B), 0.70 (d, $^3J_{H–H}$ = 6.9 Hz, 1 × –CH(CH_3)$_2$, p-cymene, conformer A). ^{13}C{^{1}H} NMR (100.613 MHz, DMSO-d_6, 298 K): δ 133.7–127.3 (unresolved m, PPh), 106.2 (br m, 1 × –C^1, p-cymene, conformer A + B), 93.1 (br m, 1 × –C^4, p-cymene, conformer A + B), 90.3 (br s, $\Delta\nu_{1/2}$ = 11.8 Hz, 2 × CH, –$C^{3,5}$–H, p-cymene, conformer A + B), 85.3 (br m, $\Delta\nu_{1/2}$ = 22.7 Hz, 2 × CH, –$C^{2,6}$–H, p-cymene, conformer A + B), 32.6 (unresolved m, PCH_2^ACH_2^BP, κ^2-dppe), 29.8 (s, CH_2, dpph), 29.7 (s, CH_2, dpph), 29.5 (br s, $\Delta\nu_{1/2}$ = 10.1 Hz, 1 × –CH(CH_3)$_2$, p-cymene, conformer A + B), 25.3–21.5 (unresolved m, 4 × CH_2, dpph), 23.4 (PCH_2^ACH_2^BP, κ^2-dppe), 20.9 (br s, $\Delta\nu_{1/2}$ = 9.8 Hz, 1 × –CH(CH_3)$_2$, p-cymene, conformer A + B), 16.9 (br m, 1 × –C(CH_3), p-cymene, conformer A + B). ^{31}P{^{1}H} NMR (161.976 MHz, DMSO-d_6, 298 K): δ 66.4–66.1 (br ps d, $\Delta\nu_{1/2}$ = 34.7 Hz, P^B, conformer A + B), 64.7 (ps dd, $^2J_{PA–PC}$ = 413.5 Hz, $^2J_{PA–PB}$ = 6.8 Hz, P^A, conformer B), 64.6 (ps dd, $^2J_{PA–PC}$ = 413.7 Hz, P^A, conformer A), 23.9 (br s, $\Delta\nu_{1/2}$ = 6.5 Hz, P^D, conformer B), 23.6 (br s, $\Delta\nu_{1/2}$ = 6.5 Hz, P^D, conformer A), 18.0 (dd, $^2J_{PC–PA}$ = 410.3 Hz, $^2J_{PC–PB}$ = 19.1 Hz, P^C, conformer B), 17.8 (dd, $^2J_{PC–PA}$ = 411.6 Hz, $^2J_{PC–PB}$ = 19.1 Hz, P^C, conformer A). ^{19}F NMR (376.498 MHz, DMSO-d_6, 298 K): δ = −77.6 (OTf). FTIR (cm^{-1}): 3054 (vw), 2920 (vw), 1434 (m), 1262 (s), 1147 (m), 1099 (m), 1030 (s), 997 (w), 743 (m), 690 (vs), 637 (vs), 530 (vs), 516 (s), 483 (s). UV/Vis λ_{max} (dichloromethane): 226 nm (major, ε = 102 476 M^{-1} cm^{-1}), 267 nm (shoulder, ε = 39 295 M^{-1} cm^{-1}), 332 nm (minor, ε = 24 133 M^{-1} cm^{-1}), 487 (weak, forbidden d–d). ESI-TOF-MS (3 kV, dichloromethane):

m/z calcd for [(κ²-dppe)PdCl(μ-dpph) RuCl₂(η⁶-p-cymene)]⁺, 1301.2; expt., 1301.1 (70%). m/z calcd for [(κ²-dppe)PdCl(κ¹-dpph)O]⁺, 1009.2; expt. 1009.1 (12%). m/z calcd for [(κ²-dppe)PdCl(κ¹-dpph)]⁺, 993.2; expt. 993.2 (100%). m/z calcd for [(κ²-dppe)PdCl]⁺, 541.0; expt., 541.0 (7%). Temperature studies: ³¹P{¹H} NMR (161.976 MHz, DMSO-d_6, 313 K): δ 66.1 (ps d, ²J_{PB-PC} = 20.3 Hz, P^B, conformer A + B), 64.7 (ps dd, ²J_{PA-PC} = 413.5 Hz, ²J_{PA-PB} = 6.8 Hz, P^A, pseudo coalescent signals), 23.7 (br s, Δ$ν_{1/2}$ = 7.7 Hz, P^D, conformer B), 23.3 (br s, Δ$ν_{1/2}$ = 6.9 Hz, P^D, conformer A), 17.9 (ps dd, ²J_{PC-PA} = 412.6 Hz, ²J_{PC-PB} = 19.5 Hz, P^C, pseudo coalescent signals). ³¹P{¹H} NMR (161.976 MHz, DMSO-d_6, 333 K): δ 66.7 (m, P^B, coalescent signals), 64.5 (ps dd, ²J_{PA-PC} = 406.3 Hz, P^A, pseudo coalescent signals), 23.4 (br s, Δ$ν_{1/2}$ = 11.4 Hz, P^D, conformer B), 23.1 (br s, Δ$ν_{1/2}$ = 7.3 Hz, P^D, conformer A), 18.2 (ps dd, ²J_{PC-PA} = 411.6 Hz, ²J_{PC-PB} = 19.5 Hz, P^C, pseudo coalescent signals). ³¹P{¹H} NMR (161.976 MHz, DMSO-d_6, 353 K): δ 65.9 (m, P^B/P^A, coalescent signals, P^A dd in baseline), 23.1 (br s, Δ$ν_{1/2}$ = 8.0 Hz, P^D, conformer B), 22.8 (br s, Δ$ν_{1/2}$ = 7.1 Hz, P^D, conformer A). ³¹P{¹H} NMR (161.976 MHz, DMSO-d_6, 373 K): δ 65.8 (m, P^B/P^A, coalescent signals, P^A dd in baseline), 22.9 (br s, Δ$ν_{1/2}$ = 7.8 Hz, P^D, conformer B), 22.7 (br s, Δ$ν_{1/2}$ = 7.4 Hz, P^D, conformer A). ³¹P{¹H} NMR (161.976 MHz, DMSO-d_6, 393 K): δ 23.4 (s, P^D, coalescent signal).

General procedure for the synthesis of [(κ²-dppe)ClPt(μ-dppx) RuCl₂(η⁶-p-cym)](OTf) (PtRu-x)

A solution of 0.123 mmol (2.00 eq.) of Pt-x in 15 mL dichloromethane was added to a solution containing 1 equivalent of [(p-cym)RuCl₂]₂ in 10 mL of dichloromethane. It was stirred at room temperature for 2 h. The solvents were removed *in vacuo* before washing with Et₂O. The resulting powder was subsequently dried *in vacuo*.

Characterisation of [(κ²-dppe)ClPt(μ-dppb)RuCl₂(η⁶-p-cym)] (OTf) (PtRu-1)

139 mg (73%) of red powder, air stable. Melting point: decomposition at 182 °C. ¹H NMR (400.130 MHz, DMSO-d_6, 293 K): δ 7.99–7.01 (40 H, unresolved m, PPh, conformer A + B), 5.43 (2 H, d, ³J_{H-H} = 5.9 Hz, 2 × CH, –C^{3,5}–H, p-cymene, conformer B), 5.36 (d, ³J_{H-H} = 6.0 Hz, 2 × CH, p-cymene, –C^{3,5}–H, conformer A), 5.22 (2 H, d, ³J_{H-H} = 6.0 Hz, 2 × CH, –C^{2,6}–H, p-cymene, conformer B), 5.17 (d, ³J_{H-H} = 6.0 Hz, 2 × CH, –C^{2,6}–H, p-cymene, conformer A), 2.71 (2 H, unresolved m, CH_2, PCH^A_2CH^B_2P, κ²-dppe, conformer A + B), 2.44 (2 H, unresolved m, CH_2, PCH^A_2CH^B_2P, κ²-dppe, conformer A + B), 2.35–2.22 (5 H, unresolved m, 2 × CH_2, dppb + 1 × –CH(CH₃)₂, p-cymene, conformer A + B), 2.08 (1 H, unresolved m, CH_2, dppb, conformer A + B), 1.78 (3 H, s, –C(CH_3), p-cymene, conformer B), 1.70 (s, –C(CH_3), p-cymene, conformer A), 1.29–1.15 (3 H, unresolved m, CH_2, dppb, conformer A + B), 0.74 (6 H, d, ³J_{H-H} = 6.9 Hz, –CH(CH_3)₂, p-cymene, conformer B), 0.69 (d, ³J_{H-H} = 6.9 Hz, –CH(CH_3)₂, p-cymene, conformer A). ¹³C{¹H} NMR (100.613 MHz, DMSO-d_6, 293 K): δ 134.0128.2 (unresolved m, PPh), 126.9 (d, $^xJ_{C-P}$ = 57.7 Hz, PPh), 124.4 (d, $^xJ_{C-P}$ = 62.3 Hz, PPh), 122.3 (s, PPh), 119.1 (s, PPh), 106.3 (s, C^1, p-cymene, con-

former A + B), 93.5 (s, C^4, p-cymene, conformer A + B), 90.2 (ps d, ²J_{H-P} = 3.9 Hz, –$C^{3,5}$–H, p-cymene, conformer A + B), 85.5 (d, ²J_{H-P} = 5.9 Hz, –$C^{2,6}$–H, p-cymene, conformer A + B), 32.8 (br s, PC^{A}H₂C^BH₂P, κ²-dppe), 29.5 (s, –CH(CH₃)₂), 26.6 (s, dppb), 24.3 (unresolved m, dppb + PC^{A}H₂C^BH₂P, κ²-dppe), 21.5 (s, dppb), 20.9 (s, –CH(CH_3)₂), 17.0 (s, –C(CH_3), p-cymene,). ³¹P{¹H} NMR (161.976 MHz, DMSO-d_6, 293 K): δ 53.8 (obscured dd, ²J_{PA-Pt} = 2377.5 Hz, ²J_{PA-PB} = 380 Hz, P^A, conformer A), 53.7 (dd, ²J_{PA-Pt} = 2377.5 Hz, ²J_{PA-PB} = 381 Hz, ²J_{PA-PB} = 5.6 Hz, P^A, conformer B), 44.8 (dd, ²J_{PB-Pt} = 3517.3 Hz, ²J_{PB-PC} = 16.2 Hz, ²J_{PB-PA} = 5.4 Hz, P^B, conformer A), 44.5 (dd, ²J_{PB-Pt} = 3509.0 Hz, ²J_{PB-PC} = 16.3 Hz, ²J_{PB-PA} = 5.6 Hz, P^B, conformer A), 23.8 (s, P^D, conformer A), 23.3 (s, P^D, conformer B), 17.2 (dd, ²J_{PC-Pt} = 2375.5 Hz, ²J_{PC-PA} = 380.4 Hz, ²J_{PC-PB} = 16.0 Hz, P^C, conformer A), 17.1 (dd, ²J_{PC-Pt} = 2375.5 Hz, ²J_{PC-PA} = 380.8 Hz, ²J_{PC-PB} = 16.3 Hz, P^C, conformer B). ¹⁹F (376.498 MHz, DMSO-d_6, 293 K): δ −77.6 (OTf). FTIR (cm⁻¹): 3055 (w), 2962 (w), 1436 (m), 1260 (s), 1147 (m), 1101 (s), 1030 (s), 999 (m), 800 (m), 744 (s), 691 (s), 637 (s), 532 (s), 517 (s), 486 (s). ESI-TOF-MS (3 kV, aceto-nitrile): m/z calcd [(κ²-dppe)PtCl(μ-dppb)RuCl₂(η⁶-p-cymene)]⁺, 1361.2; expt., 1361.3 (100%); [(κ²-dppe)PtCl (κ¹-dppb)O]⁺, 1055.2; expt., 1055.3 (54.1%); [PtCl(κ¹-dppb)]OTf-H⁺, 842.0; expt., 842.2 (86.1%).

Characterisation of [(κ²-dppe)ClPt(μ-dpppent)RuCl₂(η⁶-p-cym)] (OTf) (PtRu-2)

116 mg (61%) of red solid, air stable. ¹H NMR (400.130 MHz, DMSO-d_6, 293 K): δ 7.95–7.03 (40 H, unresolved m, PPh, conformer A + B), 5.43 (2 H, d, ³J_{H-H} = 5.40 Hz, 2 × CH, –C^{3,5}–H, p-cymene, conformer B), 5.37 (d, ³J_{H-H} = 5.30 Hz, 2 × CH, –C^{3,5}–H, p-cymene, conformer A), 5.23 (2 H, d, ³J_{H-H} = 6.10 Hz, 2 × CH, –C^{2,6}–H, p-cymene, conformer B), 5.19 (d, ³J_{H-H} = 6.10 Hz, 2 × CH, –C^{2,6}–H, p-cymene, conformer A), 2.69 (2 H, unresolved m, 1 × CH_2, PCH_2^A CH_2^B P, κ²-dppe, conformer A + B), 2.33 (6 H, unresolved m, –CH(CH₃)2 + PCH_2^A CH_2^B P, κ²-dppe + dpppent, conformer A + B), 2.15 (1 H, m, dpppent, conformer A + B), 1.77 (3 H, s, –C(CH_3), p-cymene, conformer B), 1.71 (2 H, s, –C(CH_3), p-cymene, conformer A), 1.23 (3 H, m, dpppent, conformer A + B), 1.06 (1.86 H, m, dpppent, conformer A + B), 0.74 (6 H, d, ³J_{H-H} = 6.95 Hz, –CH(CH_3)₂, p-cymene, conformer B), 0.72 (4.5 Hz, d, ³J_{H-H} = 7.05 Hz, –CH(CH_3)₂, p-cymene, conformer A). ¹³C{¹H} NMR (100.613 MHz, DMSO-d_6, 293 K): δ 133.7–127.9 (unresolved m, PPh, conformer A + B), 119.1 (s, PPh), 106.3 (s, –C^1–H, p-cymene, conformer A + B), 93.4 (s, –C^4–H, p-cymene, conformer B), 93.2 (s, –C^4–H, p-cymene, conformer A), 90.3 (unresolved m, –$C^{3,5}$–H, p-cymene, conformer A + B), 85.4 (d, ³J_{C-P} = 4.93 Hz, –$C^{2,6}$–H, p-cymene, conformer B), 85.2 (d, ³J_{C-P} = 5.39 Hz, –$C^{2,6}$–H, p-cymene, conformer A), 33.1 (unresolved m, PC^{A}H₂C^BH₂P, κ²-dppe), 31.5 (unresolved m, dpppent), 29.5 (s, –CH(CH₃)₂), 24.7 (unresolved m, dpppent + PC^{A}H₂C^BH₂P, κ²-dppe), 21.0 (s, –CH(CH_3)₂), 17.0 (s, –C(CH_3), conformer B), 16.9 (s, –C(CH_3), conformer A). ³¹P{¹H} NMR (161.976 MHz, DMSO-d_6, 293 K): δ 53.93 (overlapping dd, ²J_{PA-Pt} = 2368.6 Hz, ²J_{PA-PC} = 379.9 Hz, ²J_{PA-PB} = 5.59 Hz, P^A, conformer A), 53.89 (overlapping dd, ¹J_{PA-Pt} = 2368.6 Hz, ²J_{PA-PC} = 379.9 Hz, ²J_{PA-PB} = 5.65 Hz, P^A, conformer B), 45.04 (overlap-

ping dd, $^1J_{PB-Pt}$ = 3514.4 Hz, $^2J_{PB-PC}$ = 15.5 Hz, $^2J_{PB-PA}$ = 5.6 Hz, P^B, conformer A), 44.94 (overlapping dd, $^1J_{PB-Pt}$ = 3514.4 Hz, $^2J_{PB-PC}$ = 15.6 Hz, $^2J_{PB-PA}$ = 5.7 Hz, P^B, conformer B), 23.8 (s, P^D, conformer B), 23.3 (s, P^D, conformer A), 17.00 (dd, $^1J_{PC-Pt}$ = 2372.6 Hz, $^2J_{PC-PA}$ = 380.1 Hz, $^2J_{PC-PB}$ = 15.9 Hz, PC, conformer A), 16.87 (dd, $^2J_{PC-PB}$ = 16.2 Hz, $^2J_{PC-PA}$ = 380.2 Hz, $^1J_{PC-Pt}$ = 2372.6 Hz, P^C, conformer B). ^{19}F NMR (376.498 MHz, DMSO-d_6, 293 K): δ −77.6 (OTf). FTIR (cm^{-1}): 3055 (w), 2928 (w), 2864 (w), 1436 (m), 1261 (s), 1223 (m), 1147 (m), 1100 (m), 1030 (s), 998 (m), 744 (m), 691 (s), 636 (s), 532 (s), 517 (s), 488 (s). ESI-TOF-MS (3 kV, acetonitrile): m/z calcd [(κ^2-dppe)PtCl(μ-dppp)RuCl$_2$(η^6-p-cymene)]$^+$, 1375.2; expt., 1375.2 (67.3%); calcd [(κ^2-dppe)PtCl(κ^1-dppp)]$^+$, 1069.2; expt., 1069.3 (76.6%).

Characterisation of [(κ^2-dppe)ClPt(μ-dpph)RuCl$_2$(η^6-p-cym)] (OTf) (PtRu-3)

94 mg (74%) of red solid, air stable. ^1H NMR (400.130 MHz, DMSO-d_6, 293 K): δ 7.88–7.15 (40 H, unresolved m, PPh, conformer A + B), 5.42 (2 H, d, $^3J_{H-H}$ = 5.24 Hz, 2 × CH, −C^{3,5}–H, p-cymene, conformer B), 5.38 (d, $^3J_{H-H}$ = 5.29 Hz, 2 × CH, −C^{3,5}–H, p-cymene, conformer A), 5.22 (2 H, d, $^3J_{H-H}$ = 6.04 Hz, 2 × CH, −C^{2,6}–H, p-cymene, conformer B), 5.19 (d, $^3J_{H-H}$ = 6.14 Hz, 2 × CH, −C^{2,6}–H, p-cymene, conformer A), 2.73 (2 H, unresolved m, 1 × CH$_2$, PPh2C$H_2{}^A$CH$_2{}^B$P, κ^2-dppe, conformer A + B), 2.46 (signal obscured by solvent) (2 H, obscured m, 1 × CH$_2$, PPh2CH$_2{}^A$C$H_2{}^B$P, κ^2-dppe, conformer A + B), 2.40–2.22 (5 H, unresolved m, 2 × CH$_2$ + −CH(CH$_3$)$_2$, dpph + p-cymene, conformer A + B), 2.15 (1 H, unresolved m, 12 × CH$_2$, dpph, conformer A + B), 1.77 (3 H, s, −C(CH_3), p-cymene, conformer B), 1.73 (s, −C(CH_3), p-cymene, conformer A), 1.35–1.13 (3 H, unresolved m, 32 × CH$_2$, dpph, conformer A + B), 0.89 (4 H, ps d, $^xJ_{H-X}$ = 25 Hz, 2 × CH$_2$, dpph, conformer A + B), 0.72 (6 H, d, $^3J_{H-H}$ = 6.9 Hz, −CH(CH_3)$_2$, p-cymene, conformer B), 0.71 (d, $^3J_{H-H}$ = 6.9 Hz, −CH(CH_3)$_2$, p-cymene, conformer A). $^{13}C\{^1H\}$ NMR (100.613 MHz, acetone-d_6, 293 K): δ 135.0–128.7 (unresolved m, PPh), 107.7 (s, −C^1, p-cymene, conformer A + B), 94.8 (s, −C^4, p-cymene, conformer A + B), 91.3 (s, −C^{3,5}, p-cymene, conformer A + B), 86.7 (s, −C^{2,6}, p-cymene, conformer A + B), 34.4 (br s, PCH$_2$CH$_2$P, κ^2-dppe) 30.8 (s, dpph), 25.9 (s, −CH(CH$_3$)$_2$, p-cymene), 21.6 (s, dpph), 17.5 (s, −C(CH$_3$), p-cymene). $^{31}P\{^1H\}$ NMR (161.976 MHz, DMSO-d_6, 293 K): δ 54.0 (dd, $^1J_{PA-Pt}$ = 2366.8 Hz, $^2J_{PA-PC}$ = 380.0 Hz, $^2J_{PA-PB}$ = 5.61 Hz, P^A, conformer A), 53.9 (dd, $^1J_{PA-Pt}$ = 2366.8 Hz, $^2J_{PA-PC}$ = 380.2 Hz, $^2J_{PA-PB}$ = 5.61 Hz, P^A conformer B), 45.0 (dd, $^1J_{PB-Pt}$ = 3490.7 Hz, $^2J_{PB-PC}$ = 16.2 Hz, $^2J_{PB-PA}$ = 5.60 Hz, P^B conformer A), 44.8 (dd, $^1J_{PB-Pt}$ = 3526.4 Hz, $^2J_{PB-PC}$ = 16.3 Hz, $^2J_{PB-PA}$ = 5.60 Hz, P^B, conformer B), 24.0 (s, P^D, conformer B), 23.6 (s, P^D, conformer A), 17.1 (dd, $^1J_{PC-Pt}$ = 2366.7 Hz, $^2J_{PC-PA}$ = 379.0 Hz, $^2J_{PC-PB}$ = 16.1 Hz, P^C, conformer A), 17.0 (dd, $^1J_{PC-Pt}$ = 2366.7 Hz, $^2J_{PC-PA}$ = 380.4 Hz, $^2J_{PC-PB}$ = 16.3 Hz, P^C, conformer B). ^{19}F (376.498 MHz, acetone-d_6, 293 K): δ −78.6 (OTf). FT-IR (cm^{-1}): 3056 (w), 2928 (w), 2868 (w), 1436 (m), 1261 (s), 1223 (m), 1147 (m), 1101 (s), 1030 (s), 999 (m), 745 (m), 690 (s), 636 (s), 532 (s), 517 (s), 487 (s). UV/Vis λ_{max} (dichloromethane): 226 nm (major, ε = 199 139 M^{-1} cm^{-1}), 264 nm (shoulder, ε = 67 970 M^{-1} cm^{-1}), 363 nm (minor), 489 (weak, forbidden d–d).

ESI-TOF-MS (3 kV, acetonitrile): m/z calcd [(κ^2-dppe)PtCl(μ-dpph)RuCl$_2$(η^6-p-cymene)]$^+$, 1389.2; expt., 1389.3 (20.3%); [(κ^2-dppe)PtCl(κ^1-dpph)O]$^+$, 1099.3; expt., 1099.3 (0.53%); [(κ^2-dppe)PtCl(κ^1-dpph)]$^+$, 1083.3; expt., 1083.3 (12.9%). Temperature studies: ^1H NMR (400.130 MHz, DMSO-d_6, 313 K): δ 7.90–7.15 (40 H, unresolved m, PPh, conformer A + B), 5.40 (2 H, d, $^3J_{H-H}$ = 5.9 Hz, 2 × CH, −C^{3,5}–H, p-cymene, conformer B), 5.36 (d, $^3J_{H-H}$ = 6.0 Hz, 2 × CH, −C^{3,5}–H, p-cymene, conformer A), 5.23 (2 H, d, $^3J_{H-H}$ = 5.43 Hz, 2 × CH, −C^{2,6}–H, p-cymene, conformer B), 5.20 (d, $^3J_{H-H}$ = 5.95 Hz, 2 × CH, −C^{2,6}–H, p-cymene, conformer A), 2.73 (2 H, unresolved m, 1 × CH$_2$, PC$H_2{}^A$CH$_2{}^B$P, κ^2-dppe, conformer A + B), 2.45 (signal obscured by solvent) (2 H, obscured m, 1 × CH$_2$, PCH$_2{}^A$C$H_2{}^B$P, κ^2-dppe, conformer A + B), 2.34 (4 H, unresolved m, CH$_2$, dpph + −CH(CH$_3$)$_2$, p-cymene, conformer A + B), 2.15 (2 H, unresolved m, 1 × CH_2, dpph, conformer A + B), 1.76 (3 H, s, −C(CH_3), p-cymene, conformer B), 1.72 (s, −C(CH_3), p-cymene, conformer A), 1.37–1.13 (3 H, unresolved m, CH$_2$, dpph, conformer A + B), 0.90 (4 H, ps d, $^xJ_{H-X}$ = 17.2 Hz, 2 × CH$_2$, dpph, conformer A + B), 0.77 (6 H, d, $^3J_{H-H}$ = 6.00 Hz, −CH(CH_3)$_2$, p-cymene, conformer A + B). $^{31}P\{^1H\}$ NMR (161.976 MHz, DMSO-d_6, 313 K): δ 53.93 (dd, $^2J_{PA-PC}$ = 380.5 Hz, $^2J_{PA-PB}$ = 5.46 Hz, P^A, conformer A), 53.84 (dd, $^2J_{PA-PC}$ = 381.8 Hz, $^2J_{PA-PB}$ = 5.6 Hz, P^A, conformer B), 44.9 (dd, $^1J_{PB-Pt}$ = 3541.1 Hz, $^2J_{PB-PC}$ = 16.1 Hz, $^2J_{PB-PA}$ = 5.52 Hz, P^B conformer A), 44.7 (dd, $^1J_{PB-Pt}$ = 3541.1 Hz, $^2J_{PB-PC}$ = 16.2 Hz, $^2J_{PB-PA}$ = 5.54 Hz, P^B conformer B), 23.7 (s, P^C, conformer B), 23.3 (s, P^C, conformer A), 17.095 (pdd, $^1J_{PC-Pt}$ = 2366.2 Hz, $^2J_{PC-PA}$ = 381.6 Hz, $^2J_{PC-PB}$ = 16.3 Hz, P^C, conformer A), 17.0695 (dd, $^1J_{PC-Pt}$ = 2366.2 Hz, $^2J_{PC-PA}$ = 381.8 Hz, $^2J_{PC-PB}$ = 16.3 Hz, P^C, conformer B). ^1H NMR (400.130 MHz, DMSO-d_6, 333 K): δ 7.90–7.17 (40 H, unresolved m, PPh, conformer A + B), 5.37 (2 H, s, 2 × CH, −C^{3,5}–H, p-cymene, conformer B), 5.34 (d, $^3J_{H-H}$ = 5.7 Hz, 2 × CH, −C^{3,5}–H, p-cymene, conformer A), 5.23 (2 H, br s, $\Delta\nu_{1/2}$ = 20.79 Hz, −C^{2,6}–H, p-cymene, conformer A + B), 2.72 (2 H, unresolved m, PC$H_2{}^A$CH$_2{}^B$P, κ^2-dppe, conformer A + B), 2.35 (7 H, br s, $\Delta\nu_{1/2}$ = 36.02 Hz, 3 × CH$_2$, dpph + −CH(CH$_3$)$_2$, p-cymene + PC$H_2{}^A$CH$_2{}^B$P, κ^2-dppe, conformer A + B), 2.15 (1 H, unresolved m, CH_2, dpph, conformer A + B), 1.76 (3 H, s, −C(CH_3), p-cymene, conformer B), 1.72 (s, −C(CH_3), p-cymene, conformer A), 1.38–1.13 (3 H, unresolved m, CH_2, dpph, conformer A + B), 0.92 (4 H, unresolved m, 2 × CH_2, dpph, conformer A + B), 0.81 (6 H, s, −CH(CH_3)$_2$, p-cymene, conformer A + B). $^{31}P\{^1H\}$ NMR (161.976 MHz, DMSO-d_6, 333 K): δ 53.9 (ps dd, $^2J_{PA-PC}$ = 381.1 Hz, P^A, conformer A), 53.8 (ps dd, $^2J_{PA-PC}$ = 382.5 Hz, P^A, conformer B), 44.8 (ps dd, $^2J_{PB-PC}$ = 16.1 Hz, P^B, conformer A), 44.6 (ps dd, $^2J_{PB-PC}$ = 16.2 Hz, $^2J_{PB-PA}$ = 5.85 Hz, P^B, conformer B), 23.4 (s, P^C, conformer B), 23.1 (s, P^C, conformer A), 17.4 (dd, $^2J_{PC-PA}$ = 382.0 Hz, $^2J_{PC-PB}$ = 16.3 Hz, P^C, conformer A + B). ^1H NMR (400.130 MHz, DMSO-d_6, 353 K): δ 7.90–7.18 (40 H, unresolved m, PPh, conformer A + B), 5.34 (2 H, br s, $\Delta\nu_{1/2}$ = 21.20 Hz, −C^{3,5}–H, p-cymene, conformer A + B), 5.23 (2 H, br s, $\Delta\nu_{1/2}$ = 17.63 Hz, −C^{2,6}–H, p-cymene, conformer A + B), 2.72 (2 H, ps d, $^xJ_{H-X}$ = 31.9 Hz, PC$H_2{}^A$CH$_2{}^B$P, κ^2-dppe, conformer A + B), 2.45–2.25 (7 H, unresolved m, 3 × CH$_2$, dpph + −CH(CH$_3$)$_2$, p-cymene + PC$H_2{}^A$CH$_2{}^B$P, κ^2-dppe, conformer A +

B), 2.15 (1 H, unresolved m, CH_2, dpph, conformer A + B), 1.75 (3 H, s, –C(CH_3), *p*-cymene, conformer B), 1.72 (s, –C(CH_3), *p*-cymene, conformer A), 1.22 (3 H, unresolved m, CH_2, dpph, conformer A + B), 0.92 (4 H, 2 × CH_2, dpph, conformer A + B), 0.84 (6 H, s, –CH(CH_3)$_2$, *p*-cymene, conformer A + B). ^{31}P{^{1}H} NMR (161.976 MHz, DMSO-d_6, 353 K): δ 53.8 (ps dd, $^2J_{P^A–P^C}$ = 380.1 Hz, P^A, conformer A + B), 44.8 (resolved m, P^B, conformer A), 44.6 (dd, $^2J_{P^B–P^C}$ = 16.0 Hz, $^2J_{P^B–P^A}$ = 5.79 Hz, P^B, conformer B), 23.2 (s, P^C, conformer B), 23.1 (s, P^C, conformer A), 17.2 (ps dd, $^2J_{P^C–P^A}$ = 381.3 Hz, $^2J_{P^C–P^B}$ = 16.5 Hz, P^C, conformer A + B).

General procedure for the synthesis of [(κ^2-dppe)ClPd(μ-dppx)OsCl$_2$(η^6-*p*-cym)](OTf) (PdOs-*x*)

Two equivalents of the respective diphosphine (0.253 mmol, 2.00 eq.) were dissolved in dichloromethane (5 mL) in a Schlenk flask. Similarly, 174.4 mg (0.1265 mmol, 1.00 eq.) of **PdPd-0** was dissolved in dichloromethane (5 mL) and added dropwise to the diphosphine solution. The resulting solution was left to stir at room temperature for one hour. 100 mg (0.1265 mmol, 1.00 eq.) of [(η^6-*p*-cymene)OsCl$_2$]$_2$ dimer was dissolved in dichloromethane (5 mL), under the same conditions as above, and transferred to a Schlenk flask. The **Pd-*x*** solution was then added rapidly to the Os dimer solution while stirring. The resulting solution was left to stir at room temperature for two hours. The solvent was removed *in vacuo*, after which the resulting solid was washed with Et$_2$O (10 mL), and the washings discarded. The product was subsequently dried *in vacuo* overnight.

Characterisation of [(κ^2-dppe)ClPd(μ-dppx)OsCl$_2$(η^6-*p*-cym)] (OTf) (PdOs-1)

283 mg (74%) of grey-brown-yellow solid. Melting point: 160–165 °C (melt), 170 °C + (dec.). ^{1}H NMR (400.130 MHz, DMSO-d_6, 298 K): δ 7.84–7.11 (40 H, unresolved m, P*Ph*), 5.56 (2 H, d, $^3J_{H–H}$ = 5.8 Hz, 2 × C*H*, –C^{3,5}–*H*, *p*-cymene, conformer B), 5.50 (d, $^3J_{H–H}$ = 5.9 Hz, 2 × C*H*, –C^{3,5}–*H*, *p*-cymene, conformer A), 5.41 (2 H, d, $^3J_{H–H}$ = 5.6 Hz, 2 × C*H*, –C^{2,6}–*H*, *p*-cymene, conformer B), 5.38 (d, $^3J_{H–H}$ = 5.5 Hz, 2 × C*H*, –C^{2,6}–*H*, *p*-cymene, conformer A), 2.82 (2 H, ps d, PCH_2^{A}CH_2^{B}P, κ^2-dppe), 2.45–2.26 (obscured by solvent) (4 H, obscured m, PCH_2^{A}CH_2^{B}P, κ^2-dppe + 1 × CH_2, dppb), 2.15 (1 H, ps sept, $^3J_{H–H}$ = 6.7 Hz, 1 × –C*H*(CH$_3$)$_2$, *p*-cymene), 1.90 (2 H, unresolved m, 1 × CH_2, dppb), 1.88 (3 H, br s, $\Delta\nu_{1/2}$ = 3.6 Hz, –C(C*H$_3$*), *p*-cymene, conformer B), 1.82 (br s, $\Delta\nu_{1/2}$ = 3.3 Hz, –C(C*H$_3$*), *p*-cymene, conformer A), 1.33–1.13 (2 H, br m, 1 × CH_2, dppb), 0.98–0.84 (2 H, br m, 1 × CH_2, dppb), 0.79 (6 H, br d, $\Delta\nu_{1/2}$ = 2.8 Hz, $^3J_{H–H}$ = 6.8 Hz, –CH(C*H$_3$*)$_2$, *p*-cymene, conformer A), 0.75 (br d, $\Delta\nu_{1/2}$ = 2.7 Hz, $^3J_{H–H}$ = 6.8 Hz, –CH(C*H$_3$*)$_2$, *p*-cymene, conformer B). ^{13}C{^{1}H} NMR (100.613 MHz, DMSO-d_6, 298 K): δ 133.9–127.1 (unresolved m, P*Ph*), 97.2 (s, –C^1, *p*-cymene, conformer A + B), 86.0 (s, –C^4, *p*-cymene, conformer B), 85.7 (s, –C^4, *p*-cymene, conformer A), 81.9 (br s, $\Delta\nu_{1/2}$ = 12.4 Hz, –C^{3,5}–H, *p*-cymene, conformer A + B), 78.0 (br s, $\Delta\nu_{1/2}$ = 15.6 Hz, –C^{2,6}–H, *p*-cymene, conformer B), 77.8 (br s, $\Delta\nu_{1/2}$ = 8.7 Hz, –C^{2,6}–H, *p*-cymene, conformer A), 32.6 (ps d, $^1J_{C–P}$ = 45.0 Hz,

PCH_2^{A}CH_2^{B}P, κ^2-dppe), 29.3 (br s, $\Delta\nu_{1/2}$ = 13.2 Hz, –CH(CH$_3$)$_2$, *p*-cymene, conformer A + B), 26.2 (1 × CH_2, dppb), 24.2 (1 × CH_2, dppb), 23.9 (1 × CH_2, dppb), 22.2 (PCH_2^{A}CH_2^{B}P, κ^2-dppe), 21.8 (1 × CH_2, dppb), 21.3 (br s, $\Delta\nu_{1/2}$ = 10.0 Hz, –CH(CH$_3$)$_2$, *p*-cymene, conformer A + B), 16.8 (br m, –C(CH$_3$), *p*-cymene, conformer A + B). ^{31}P{^{1}H} NMR (161.976 MHz, DMSO-d_6, 298 K): δ 66.2–65.9 (unresolved m, P^B, conformer A + B), 64.7 (ps dd, $^2J_{P^A–P^C}$ = 385.5 Hz, $^2J_{P^A–P^B}$ = 7.8 Hz, P^A, conformer B), 64.5 (ps dd, $^2J_{P^A–P^C}$ = 397.0 Hz, $^2J_{P^A–P^B}$ = 7.4 Hz, P^A, conformer A), 17.9 (dd, $^2J_{P^C–P^A}$ = 412.4 Hz, $^2J_{P^C–P^B}$ = 20.4 Hz, P^C, conformer B), 17.8 (dd, $^2J_{P^C–P^A}$ = 411.8 Hz, $^2J_{P^C–P^B}$ = 20.7 Hz, P^C, conformer A), –17.8 (br s, $\Delta\nu_{1/2}$ = 7.0 Hz, P^D, conformer B), –18.4 (br s, $\Delta\nu_{1/2}$ = 6.9 Hz P^D, conformer A). ^{19}F NMR (376.498 MHz, DMSO-d$_6$, 298 K): δ –77.6 (OTf). FTIR (cm^{-1}): 3054 (vw), 2960 (vw), 1436 (m), 1260 (s), 1148 (m), 1099 (m), 1030 (s), 999 (w), 743 (m), 690 (vs), 637 (vs), 530 (vs), 516 (vs), 483 (s). UV/Vis λ_{max} (dichloromethane): 226 nm (major, ε = 133 371 M^{-1} cm^{-1}), 267 nm (shoulder, ε = 47 219 M^{-1} cm^{-1}), 332 nm (minor ε = 35 676 M^{-1} cm^{-1}), 421 (weak, forbidden d–d). ESI-TOF-MS (3 kV, dichloromethane): *m*/*z* calcd for [(κ^2-dppe)PdCl(μ-dppb)OsCl$_2$(η^6-*p*-cymene)]$^+$, 1361.2; expt. 1361.7 (26%). *m*/*z* calcd for [(κ^2-dppe)PdCl(κ^1-dppb)]$^+$, 965.2; expt. 965.5 (46%). *m*/*z* calcd for [(η^6-*p*-cymene)OsCl(κ^1-dppb)]$^+$, 787.2; expt. 787.5 (100%). *m*/*z* calcd for [(κ^2-dppe)PdCl]$^+$, 541.0; expt., 541.2 (3%).

Characterisation of [(κ^2-dppe)ClPd(μ-dppx)OsCl$_2$(η^6-*p*-cym)] (OTf) (PdOs-2)

311 mg (81%) of brown-yellow (turmeric) solid, air stable. ^{1}H NMR (400.130 MHz, DMSO-d_6, 298 K): δ 7.84–7.12 (40 H, unresolved m, P*Ph*), 5.56 (2 H, d, $^3J_{H–H}$ = 5.7 Hz, –C^{3,5}–*H*, *p*-cymene, conformer B), 5.51 (d, $^3J_{H–H}$ = 5.8 Hz, –C^{3,5}–*H*, *p*-cymene, conformer A), 5.43 (2 H, d, $^3J_{H–H}$ = 5.8 Hz, –C^{2,6}–*H*, *p*-cymene, conformer B), 5.39 (d, $^3J_{H–H}$ = 6.0 Hz, –C^{2,6}–*H*, *p*-cymene, conformer A), 2.81 (2 H, br m, PCH_2^{A}CH_2^{B}P, κ^2-dppe), 2.48 (obscured by solvent) (2 H, obscured br m, PCH_2^{A}CH_2^{B}P, κ^2-dppe), 2.41–2.03 (5 H, unresolved m (ps sept.), 2 × CH_2, dppp + 1 × –CH(CH$_3$)$_2$ + *p*-cymene), 1.87 (3 H, s, 1 × –C(C*H$_3$*), *p*-cymene, conformer B), 1.83 (s, 1 × –C(C*H$_3$*), *p*-cymene, conformer A), 1.25–0.83 (6 H, unresolved m, 3 × CH_2, dppp), 0.80 (6 H, ps d, $^3J_{H–H}$ = 7.0 Hz, CH(C*H$_3$*)$_2$, *p*-cymene, conformer B), 0.78 (ps d, $^3J_{H–H}$ = 7.0 Hz, –CH(C*H$_3$*)$_2$, *p*-cymene, conformer A). ^{13}C{^{1}H} NMR (100.613 MHz, DMSO-d_6, 298 K): δ 133.7–127.4 (unresolved m, P*Ph*), 97.3 (s, –C^1, *p*-cymene, conformer A + B), 85.9 (s, –C^4, *p*-cymene, conformer B), 85.7 (s, –C^4, *p*-cymene, conformer A), 81.9 (br m, $\Delta\nu_{1/2}$ = 7.4 Hz, –C^{3,5}–H, *p*-cymene, conformer A + B), 77.9 (ps d, –C^{2,6}–H, *p*-cymene, conformer B), 77.7 (ps d, $^2J_{C–P}$ = 5.2 Hz, –C^{2,6}–H, *p*-cymene, conformer A), 32.6 (PCH_2^{A}CH_2^{B}P, κ^2-dppe), 31.3 (1 × CH_2, dppp), 29.2 (br s, $\Delta\nu_{1/2}$ = 2.84 Hz, –CH(CH$_3$)$_2$, *p*-cymene, conformer A + B), 24.7 (1 × CH_2, dppp), 24.6 (1 × CH_2, dppp), 22.2 (PCH_2^{A}CH_2^{B}P, κ^2-dppe), 21.9 (1 × CH_2, dppp), 21.4 (br s, $\Delta\nu_{1/2}$ = 1.5 Hz, –CH(CH$_3$)$_2$, *p*-cymene, conformer A + B), 16.8 (s, –C(CH$_3$), *p*-cymene, conformer B), 16.7 (s, –C(CH$_3$), *p*-cymene, conformer A). ^{31}P{^{1}H} NMR (161.976 MHz, DMSO-d_6, 298 K): δ 66.3 (ps dd (hidden by conformer A), P^B, conformer B), 66.2 (dd, $^2J_{P^B–P^C}$ = 19.3 Hz,

$^2J_{PB-PA}$ = 7.6 Hz, P^B, conformer A), 64.7 (ps dd, $^2J_{PA-PC}$ = 410.7 Hz, P^A, conformer B), 64.6 (dd, $^2J_{PA-PC}$ = 411.3 Hz, $^2J_{PA-PB}$ = 7.7 Hz, P^A, conformer A), 17.8 (dd, $^2J_{PC-PA}$ = 411.0 Hz, $^2J_{PC-PB}$ = 18.8 Hz, P^C, conformer B), 17.7 (dd, $^2J_{PC-PA}$ = 411.0 Hz, $^2J_{PC-PB}$ = 18.8 Hz, P^C, conformer A), −17.9 (s, P^D, conformer B), −18.4 (s, P^D, conformer A). ^{19}F NMR (376.498 MHz, DMSO-d_6, 298 K): δ −77.6 (OTf). FT-IR (cm^{-1}): 3055 (vw), 2927 (vw), 1434 (m), 1262 (s), 1147 (m), 1099 (m), 1030 (s), 997 (w), 743 (m), 690 (vs), 637 (vs), 530 (vs), 516 (s), 481 (m). UV/Vis λ_{max} (dichloromethane): 226 (major), 270 (shoulder), 331 (minor), 430 (weak, forbidden d–d). ESI-TOF-MS (3 kV, dichloromethane): m/z calcd for [(κ^2-dppe)PdCl(μ-dppp)OsCl$_2$(η^6-p-cymene)]$^+$, 1375.2; expt., 1375.1 (78%). m/z calcd for [(κ^2-dppe)PdCl(κ^1-dppp)]$^+$, 979.2; expt. 979.2 (100%). m/z calcd for [(η^6-p-cymene)OsCl(κ^1-dppp)]$^+$, 801.2; expt. 801.2 (7%). m/z calcd for [(κ^2-dppe)PdCl]$^+$, 541.0; expt., 541.0 (60%).

Characterisation of [(κ^2-dppe)ClPd(μ-dppx)OsCl$_2$(η^6-p-cym)] (OTf) (PdOs-3)

318 mg (82%) of golden-orange solid, air stable. ^{1}H NMR (400.130 MHz, DMSO-d_6, 298 K): δ 7.84–7.16 (40 H, unresolved m, PPh), 5.56 (2 H, d, $^3J_{H-H}$ = 5.7 Hz, −C^{3,5}−H, p-cymene, conformer B), 5.52 (d, $^3J_{H-H}$ = 5.8 Hz, −C^{3,5}−H, conformer A), 5.42 (2 H, d, $^3J_{H-H}$ = 5.1 Hz, −C^{2,6}−H, p-cymene, conformer B), 5.39 (d, $^3J_{H-H}$ = 5.8 Hz, −C^{2,6}−H, p-cymene, conformer A), 2.83 (2 H, br m, PCH_2^ACH_2^BP, κ^2-dppe), 2.47 (obscured by solvent) (2 H, obscured br m, PCH_2^ACH_2^BP, κ^2-dppe), 2.35–1.89 (5 H, unresolved m (ps sept.), 2 × CH_2, dpph + −CH(CH$_3$)$_2$, p-cymene), 1.87 (3 H, s, −C(CH_3), p-cymene, conformer B), 1.84 (s, −C(CH_3), p-cymene, conformer A), 1.36–0.84 (8 H, unresolved m, 4 × CH_2, dpph), 0.78 (6 H, br d, $\Delta\nu_{1/2}$ = 11.6 Hz, −CH(CH_3)$_2$, p-cymene, conformer A + B). ^{13}C{^{1}H} NMR (100.613 MHz, DMSO-d_6, 298 K): δ 133.7–127.4 (unresolved m, PPh), 97.2 (s, −C^1, p-cymene, conformer A + B), 85.5 (s, −C^4, p-cymene, conformer A + B), 82.0 (br m, $\Delta\nu_{1/2}$ = 8.3 Hz, $C^{3,5}$, p-cymene, conformer A + B), 77.9 (m, −$C^{2,6}$, p-cymene, conformer A + B), 32.6 (PCH_2^ACH_2^BP, κ^2-dppe), 29.8 (s, 1 × CH_2, dpph), 29.7 (s, 1 × CH_2, dpph), 29.2 (br s, $\Delta\nu_{1/2}$ = 3.3 Hz, −CH(CH$_3$)$_2$, p-cymene, conformer A + B), 26.5 (1 × CH_2, dpph), 25.2 (1 × CH_2, dpph), 24.7 (1 × CH_2, dpph), 24.4 (1 × CH_2, dpph), 22.1 (PCH_2^ACH_2^BP, κ^2-dppe), 21.3 (br s, $\Delta\nu_{1/2}$ = 2.9 Hz, −CH(CH_3)$_2$, p-cymene, conformer A + B), 16.81 (s, −C(CH_3), p-cymene, conformer B), 16.76 (s, −C(CH_3), p-cymene, conformer A). ^{31}P{^{1}H} NMR (161.976 MHz, DMSO-d_6, 298 K): δ 66.4–66.1 (br m, $\Delta\nu_{1/2}$ = 37.3 Hz, P^B, conformer A + B), 64.8 (ps dd, $^2J_{PA-PC}$ = 412.3 Hz, $^2J_{PA-PB}$ = 7.4 Hz, P^A, conformer B), 64.6 (ps dd, $^2J_{PA-PC}$ = 415.0 Hz, P^A, conformer A), 18.0 (dd, $^2J_{PC-PA}$ = 410.7 Hz, $^2J_{PC-PB}$ = 19.3 Hz, P^C, conformer B), 17.9 (dd, $^2J_{PC-PA}$ = 411.3 Hz, $^2J_{PC-PB}$ = 19.4 Hz, P^C, conformer A), −17.7 (br s, $\Delta\nu_{1/2}$ = 6.8 Hz, P^D, conformer B), −18.1 (br s, $\Delta\nu_{1/2}$ = 6.2 Hz, P^D, conformer A). ^{19}F NMR (376.498 MHz, DMSO-d_6, 298 K): δ −77.6 (OTf). FT-IR (cm^{-1}): 3054 (vw), 2930 (vw), 1434 (m), 1263 (s), 1148 (w), 1099 (m), 1030 (s), 998 (w), 743 (m), 691 (vs), 637 (vs), 530 (vs), 516 (s), 486 (m). UV/Vis λ_{max} (dichloromethane): 267 nm (shoulder, ε = 51 010 M^{-1} cm^{-1}), 331 nm (minor ε = 37 695 M^{-1} cm^{-1}), 421 (weak, forbidden d–d). ESI-TOF-MS (3 kV, dichloromethane):

m/z calcd for [(κ^2-dppe)PdCl(μ-dpph)OsCl$_2$(η^6-p-cymene)]$^+$, 1389.2; expt., 1389.1 (33%). m/z calcd for [(κ^2-dppe)PdCl(μ-dpph)O]$^+$, 1009.2; expt., 1009.1 (8%). m/z calcd for [(κ^2-dppe)PdCl(κ^1-dpph)]$^+$, 993.1; expt. 993.1 (100%). m/z calcd for [(η^6-p-cymene)OsCl(κ^1-dpph)]$^+$, 815.2; expt. 815.2 (35%). m/z calcd for [(κ^2-dppe)PdCl]$^+$, 541.0; expt. 541.0 (12%).

Cell viability assays

The effect of all complexes on the viability of various human cancer cell lines was evaluated using the 3-(4,5-dimethylthiazol-2-yl)-2,5-diphenyltrazolium bromide (MTT) assay (11465007001; Sigma Aldrich, Missouri, USA) following the manufacturer's instructions. Briefly, cells were seeded in 96-well plates at low densities of 3000–10 000 and incubated for 24 to 48 hours. After incubation, cells were treated with vehicle, and all ligands and complexes at 10 μM, and the clinically approved cisplatin drug (CDDP, 10 μM) for 48 hours. Following treatment, 10 μl of MTT solution was added to each well, and the plates were incubated at 37 °C for 4 hours. The resulting purple formazan crystals were solubilised by adding 100 μl of solubilising reagent to each well. Absorbance was measured at 600 nm using a Glomax® microplate spectrophotometer. The cytotoxic effect of each complex was quantified based on the percentage inhibition of cell viability compared to the vehicle-treated control. At least three independent experiments were performed in quadruplicate to determine the IC$_{50}$ concentration of the respective complexes. The IC$_{50}$ values were calculated from sigmoidal plots with GraphPad Prism version 7.0 (GraphPad Software, California, USA).

Author contributions

B. R. – conceptualisation, data curation, formal analysis, investigation, methodology, software, validation, visualisation, writing – original draft, writing – review and editing. T. B., M. P., L. W. M., K. S., M. V. M., T. T. M., C. M. – data curation, investigation, methodology, resources, validation, visualisation, writing – review and editing. S. P., T. J. C. – funding acquisition, project administration, supervision. B. B. – conceptualisation, data curation, formal analysis, funding acquisition, methodology, project administration, resources, supervision, validation, writing – review and editing.

Conflicts of interest

There are no conflicts to declare.

Data availability

Supplementary information (SI): Experimental procedures and full characterisation of the complexes, including all spectra and X-ray data; detailed biological studies information. See DOI: https://doi.org/10.1039/d5dt02044a.

CCDC 2470481–2470483 contain the supplementary crystallographic data for this paper.[68a–c]

References

1 R. L. Siegel, T. B. Kratzer, A. N. Giaquinto, H. Sung and A. Jemal, *CA Cancer J. Clin.*, 2025, **75**, 10–45.

2 F. Bray, M. Laversanne, H. Sung, J. Ferlay, R. L. Siegel, I. Soerjomataram and A. Jemal, *CA Cancer J. Clin.*, 2024, **74**, 229–263.

3 M. Peyrone, *Justus Liebigs Ann. Chem.*, 1844, **51**, 1–29.

4 B. Rosenberg, L. Van Camp and T. Krigas, *Nature*, 1965, **205**, 698–699.

5 L. Kelland, *Nat. Rev. Cancer*, 2007, **7**, 573–584.

6 G. Y. Ho, N. Woodward and J. I. G. Coward, *Crit. Rev. Oncol. Hematol.*, 2016, **102**, 37–46.

7 T. Alcindor and N. Beauger, *Curr. Oncol.*, 2011, **18**, 18–25.

8 M. Shimada, H. Itamochi and J. Kigawa, *Cancer Manage. Res.*, 2013, **5**, 67–76.

9 G. Mestroni, E. Alessio and G. Sava, SIGEA S.R.L., World Intellectual Property Organization (WIPO), WO9800431, 1998.

10 B. K. Keppler, Deutsches Patentamt, DE19612291, 1997.

11 B. K. Keppler, M. Henn, U. M. Juhl, M. R. Berger, R. Niebl and F. E. Wagner, New ruthenium complexes for the treatment of cancer, in *Progress in clinical biochemistry and medicine*, 1989, pp. 41–69.

12 S. McFarland, Theralase INC., World Intellectual Property Organization (WIPO), WO2013158550, 2013.

13 C. S. Allardyce, P. J. Dyson, D. J. Ellis and S. L. Heath, *Chem. Commun.*, 2001, 1396–1397.

14 B. S. Murray, M. V. Babak, C. G. Hartinger and P. J. Dyson, *Coord. Chem. Rev.*, 2016, **306**, 86–114.

15 R. E. Morris, R. E. Aird, P. del Socorro Murdoch, H. Chen, J. Cummings, N. D. Hughes, S. Parsons, A. Parkin, G. Boyd, D. I. Jodrell and P. J. Sadler, *J. Med. Chem.*, 2001, **44**, 3616–3621.

16 R. E. Aird, J. Cummings, A. A. Ritchie, M. Muir, R. E. Morris, H. Chen, P. J. Sadler and D. I. Jodrell, *Br. J. Cancer*, 2002, **86**, 1652–1657.

17 T. Kuijpers and B. Blom, *Eur. J. Med. Chem.*, 2021, **223**, 113651.

18 B. Roufosse, C. Serbu, C. Marschner, S. Prince and B. Blom, *Eur. J. Med. Chem.*, 2024, **274**, 116528.

19 M. Odachowski, C. Marschner and B. Blom, *Eur. J. Med. Chem.*, 2020, **204**, 112613.

20 T. Nabiyeva, C. Marschner and B. Blom, *Eur. J. Med. Chem.*, 2020, **201**, 112483.

21 J. Bennett, A. D. Rae, G. Salem, N. C. Ward, P. Waring, K. Wells and A. C. Willis, *J. Chem. Soc., Dalton Trans.*, 2002, 234–243.

22 F. A. Serrano, A. L. Matsuo, P. T. Monteforte, A. Bechara, S. S. Smaili, D. P. Santana, T. Rodrigues, F. V. Pereira, L. S. Silva, J. Machado, E. L. Santos, J. B. Pesquero, R. M. Martins, L. R. Travassos, A. C. F. Caires and E. G. Rodrigues, *BMC Cancer*, 2011, **11**, 296.

23 A. van Niekerk, A. Blanckenberg, S. Kimani, S. Chakraborty, S. Prince, P. Chellan and S. Mapolie, *J. Inorg. Biochem.*, 2023, **243**, 112191.

24 W. Villarreal, L. Colina-Vegas, C. Rodrigues de Oliveira, J. C. Tenorio, J. Ellena, F. C. Gozzo, M. R. Cominetti, A. G. Ferreira, M. A. B. Ferreira, M. Navarro and A. A. Batista, *Inorg. Chem.*, 2015, **54**, 11709–11720.

25 V. T. Yilmaz, C. Icsel, M. Aygun, M. Erkisa and E. Ulukaya, *Eur. J. Med. Chem.*, 2018, **158**, 534–547.

26 C. Cullinane, G. B. Deacon, P. R. Drago, A. P. Erven, P. C. Junk, J. Luu, G. Meyer, S. Schmitz, I. Ott, J. Schur, L. K. Webster and A. Klein, *Dalton Trans.*, 2018, **47**, 1918–1932.

27 C. Icsel, V. T. Yilmaz, M. Aygun, B. Cevatemre, P. Alper and E. Ulukaya, *Dalton Trans.*, 2018, **47**, 11397–11410.

28 J. L. Dutra, J. Honorato, A. Graminha, C. A. F. Moraes, K. T. de Oliveira, M. R. Cominetti, E. E. Castellano and A. A. Batista, *Dalton Trans.*, 2024, **53**, 18902–18916.

29 G. Tonon, M. Mauceri, E. Cavarzerani, R. Piccolo, C. Santo, N. Demitri, L. Orian, P. A. Nogara, J. B. T. Rocha, V. Canzonieri, F. Rizzolio, F. Visentin and T. Scattolin, *Dalton Trans.*, 2024, **53**, 8463–8477.

30 R. Czarnomysy, D. Radomska, O. K. Szewczyk, P. Roszczenko and K. Bielawski, *Int. J. Mol. Sci.*, 2021, **22**, 8271.

31 T. Scattolin, V. A. Voloshkin, F. Visentin and S. P. Nolan, *Cell Rep. Phys. Sci.*, 2021, **2**, 100446.

32 C. Zhang, C. Xu, X. Gao and Q. Yao, *Theranostics*, 2022, **12**, 2115–2132.

33 D. Sahoo, P. Deb, T. Basu, S. Bardhan, S. Patra and P. K. Sukul, *Bioorg. Med. Chem.*, 2024, **112**, 117894.

34 S. Das, S. Sinha, R. Britto, K. Somasundaram and A. G. Samuelson, *J. Inorg. Biochem.*, 2010, **104**, 93–104.

35 B. Herry, L. K. Batchelor, B. Roufosse, D. Romano, J. Baumgartner, M. Borzova, T. Reifenstahl, T. Collins,

A. Benamrane, J. Weggelaar, M. C. Correia, P. J. Dyson and B. Blom, *J. Organomet. Chem.*, 2019, **901**, 120934.

36 E. Klaimanee, T. Nhukeaw, S. Saithong, A. Ratanaphan, S. Phongpaichit, Y. Tantirungrotechai and N. Leesakul, *Polyhedron*, 2021, **204**, 115244.

37 H. R. Shahsavari, N. Giménez, E. Lalinde, M. T. Moreno, M. Fereidoonnezhad, R. B. Aghakhanpour, M. Khatami, F. Kalantari, Z. Jamshidi and M. Mohammadpour, *Eur. J. Inorg. Chem.*, 2019, **2019**, 1360–1373.

38 M. Odachowski, R. Neven, G. Perversi, D. Romano, C. A. Slabber, M. Hadiji, M. Honing, Y. Zhao, O. Q. Munro and B. Blom, *J. Inorg. Biochem.*, 2023, **242**, 112156.

39 B. Tűz, I. Correia and P. N. Martinho, *J. Inorg. Biochem.*, 2025, **264**, 112813.

40 E. Giorgi, F. Binacchi, C. Marotta, D. Cirri, C. Gabbiani and A. Pratesi, *Molecules*, 2023, **28**, 273.

41 J. A. Davies, F. R. Hartley and S. G. Murray, *J. Chem. Soc., Dalton Trans.*, 1979, 1705–1708, DOI: [10.1039/DT9790001705](10.1039/DT9790001705).

42 J. A. Davies, F. R. Hartley and S. G. Murray, *Inorg. Chem.*, 1980, **19**, 2299–2303.

43 F. R. Hartley, S. G. Murray and A. Wilkinson, *Inorg. Chem.*, 1989, **28**, 549–554.

44 J. S. Kumar, A. K. Singh, J. Yang and J. E. Drake, *J. Coord. Chem.*, 1998, **44**, 335–342.

45 A. S. Abu-Surrah, T. Debaerdemaeker, W. Huhn, B. Rieger, M. Klinga, T. Repo and M. Leskelä, *Acta Crystallogr. Sect. C*, 2000, **56**, e42–e43.

46 Y. Zhou, X. Xu, H. Sun, G. Tao, X.-Y. Chang, X. Xing, B. Chen and C. Xu, *Nat. Commun.*, 2021, **12**, 1953.

47 F. E. Hahn, D. Klusmann and T. Pape, *Eur. J. Inorg. Chem.*, 2008, **2008**, 4420–4424.

48 G. Berton, T. Lorenzetto, G. Borsato, P. Sgarbossa, C. Santo, F. Visentin, F. Fabris and A. Scarso, *Tetrahedron Lett.*, 2019, **60**, 151202.

49 P. A. W. Dean, J. J. Vittal and R. S. Srivastava, *Can. J. Chem.*, 1987, **65**, 2628–2633.

50 T. Grell, P. Wonneberger, D. M. Yufanyi, P. Lönnecke and E. Hey-Hawkins, *Chem. – Eur. J.*, 2025, **31**, e202500746.

51 J. W. Faller and N. Sarantopoulos, *J. Organomet. Chem.*, 2023, **1000**, 122846.

52 Y. Otero, D. Peña, A. Arce, M. Hissler, R. Réau, Y. De Sanctis, E. Ocando-Mavárez, R. Machado and T. González, *J. Organomet. Chem.*, 2015, **799–800**, 45–53.

53 C. Gourlaouen, F. Elaieb, E. Brenner, D. Matt, J. Harrowfield and L. Ricard, *Dalton Trans.*, 2023, **52**, 9202–9207.

54 M. A. Zhuravel, D. S. Glueck, C. D. Incarvito and A. L. Rheingold, *Organometallics*, 1999, **18**, 4673–4676.

55 J. Bruckmann and C. Krüger, *J. Organomet. Chem.*, 1997, **536–537**, 465–472.

56 A. B. Chaplin and P. J. Dyson, *Eur. J. Inorg. Chem.*, 2007, **2007**, 4973–4979.

57 O. Volkov, N. P. Rath and L. Barton, *Organometallics*, 2002, **21**, 5505–5514.

58 J. Fernández-Gallardo, B. T. Elie, M. Sanaú and M. Contel, *Chem. Commun.*, 2016, **52**, 3155–3158.

59 V. Cadierno, P. Crochet, J. Díez, J. García-Álvarez, S. E. García-Garrido, J. Gimeno, S. García-Granda and M. A. Rodríguez, *Inorg. Chem.*, 2003, **42**, 3293–3307.

60 M. R. Boyd and K. D. Paull, *Drug Dev. Res.*, 1995, **34**, 91–109.

61 A. M. Burger and H. H. Fiebig, Preclinical screening for new anticancer agents, in *Handbook of Anticancer Pharmacokinetics and Pharmacodynamics, Cancer drug discovery and development*, 2014, pp. 23–38.

62 A. Welsh, K. Serala, S. Prince and G. S. Smith, *J. Med. Chem.*, 2024, **67**, 6673–6686.

63 W. Yang, J. Soares, P. Greninger, E. J. Edelman, H. Lightfoot, S. Forbes, N. Bindal, D. Beare, J. A. Smith, I. R. Thompson, S. Ramaswamy, P. A. Futreal, D. A. Haber, M. R. Stratton, C. Benes, U. McDermott and M. J. Garnett, *Nucleic Acids Res.*, 2012, **41**, D955–D961.

64 E. Stefàno, L. G. Cossa, F. De Castro, E. De Luca, V. Vergaro, G. My, G. Rovito, D. Migoni, A. Muscella, S. Marsigliante, M. Benedetti and F. P. Fanizzi, *Bioinorg. Chem. Appl.*, 2023, **2023**, 1–14.

65 Ž. D. Bugarčić, J. Bogojeski and R. van Eldik, *Coord. Chem. Rev.*, 2015, **292**, 91–106.

66 S. Dasari and P. B. Tchounwou, *Eur. J. Pharmacol.*, 2014, **740**, 364–378.

67 R. Castarlenas, M. A. Esteruelas and E. Oñate, *Organometallics*, 2005, **24**, 4343–4346.

68 (*a*) CCDC 2470481: Experimental Crystal Structure Determination, 2025, DOI: 10.5517/ccdc.csd.cc2nxqy8; (*b*) CCDC 2470482: Experimental Crystal Structure Determination, 2025, DOI: 10.5517/ccdc.csd.cc2nxqz9; (*c*) CCDC 2470483: Experimental Crystal Structure Determination, 2025, DOI: 10.5517/ccdc.csd.cc2nxr0c.